Technical Report 78-49

DEVELOPMENT OF IMPROVED LITHIUM TANTALATE PYROELECTRIC DETECTORS

N. E. Byer, A. Van der Jagt, W. Holton

Submitted to

National Aeronautics and
Space Administration
Langley Research Center
Hampton, Virginia 23665

Martin Marietta Corporation
Martin Marietta Laboratories
1450 South Rolling Road
Baltimore, Maryland 21227

November 1978

TABLE OF CONTENTS

LIST OF TABLES

LIST OF FIGURES

DEVELOPMENT OF IMPROVED LITHIUM TANTALATE PYROELECTRIC DETECTORS

N. E. Byer, A. Van der Jagt, W. Holton

Martin Marietta Corporation
Martin Marietta Laboratories

SUMMARY

A program was undertaken to increase the detectivity of $LiTaO_3$ pyroelectric detectors to meet a performance requirement D* (500 K, 15 Hz) = 4 x 10^9 cmHz$^{1/2}$W^{-1}. To attain this goal, emphasis was placed on 1) reduction of the thermal conductance of the detector element to its surroundings; 2) thinning the detector wafer to a thickness less than 3 μm; and 3) increasing the absorptivity of the standard metallic film coatings.

During the course of the program, thermal conductance was reduced by 41% through the use of a reticulated, i.e., slotted, structure. By means of ion milling techniques, self-supported detector wafers less than 2 μm thick were fabricated. Multiple layer coatings, including an AR coating, with 16% improvements in absorptance were designed and fabricated. However, later refinements in the multilayer design program led to construction of detectors with absorptivities of 75-80%. Because of a mismatch in the thermal expansion coefficients between the AR coatings and $LiTaO_3$, detectors with these coatings had to be more than 2 μm thick.

Three assemblies were constructed and delivered. These units consisted of the detector chip and a hybrid JFET preamplifier sealed in an evacuable header with a germanium window. An evacuation valve was provided for experiments in various atmospheres. Because the AR coatings were not available until late in the program, the detectors employed in these units were fitted with standard nichrome coatings.

A D* (500 K, 15 Hz) of 1.34 x 10^9 cmHz$^{1/2}$W^{-1} was achieved in a vacuum ambient. Vibrational sensitivities of 20-60 μV/g were measured, which are comparable to those of unreticulated devices.

Based on process and design improvements developed during this program, detectivities of 2.5 x 10^9 cmHz$^{1/2}$W^{-1} can be contemplated. However, practical $LiTaO_3$ detectors with still larger detectivities are considered unlikely.

INTRODUCTION

The need for uncooled, inexpensive infrared detectors has stimulated the development of thermal detectors based on the pyroelectric effect. From earlier work directed toward finding suitable pyroelectric materials, four materials have emerged as useful for practical pyroelectric detectors (PEDs): triglycine sulfate (TGS) and its isomorphs, lithium tantalate ($LiTaO_3$), strontium barium niobate (SBN), and polyvinylidene difluoride (PVF_2) (refs. 1-4). Detectors fabricated from the first three materials have attained normalized detectivities, D*, of 10^9 $cmHz^{1/2}W^{-1}$ (with noise equivalent powers, NEP, of $10^{-10}WHz^{-1/2}$) -- much greater than the 10^8 $cmHz^{1/2}W^{-1}$ values for D* prevalent over a decade ago, but still significantly less than the radiative limit of 2×10^{10} $cmHz^{1/2}W^{-1}$ (refs. 5-7).

At Martin Marietta Laboratories, we have focused our efforts on $LiTaO_3$ because of its following attributes:

- Wide storage and operating temperature range
  - Curie temperature: 610°C
  - Poling voltage not required
- High coercive field
  - Accidental depoling unlikely
- Non-hydroscopic
  - Storage in air, inert gas, or vacuum
- Good figure of merit
  - High voltage responsivity
- Low dielectric loss
- Low piezoelectric sensitivity

- High mechanical strength
- Compatibility with wafer processing techniques
  - Ion-beam milling
  - Photolithography
- Ready availability.

Therefore, the purpose of this contract, NAS1-15106, was to increase the detectivity of $LiTaO_3$ detectors to a level suitable for a larger number of NASA's infrared detector requirements. Accordingly, our goal was to fabricate and deliver three detector/preamplifier assemblies with detectivities of 4×10^9 $cmHz^{1/2}W^{-1}$ as measured with a 500 K black-body source and a 15-Hz chopping frequency.

This final report summarizes the work that has been done on the program. Detector and preamplifier design are discussed first. Subsequent sections detail the fabrication and assembly techniques; test results for the detectors, preamplifiers, and detector assemblies; and factors limiting D*. In particular, the thermal component of dielectric loss, which contributes the major noise source, i.e., temperature noise, is analyzed. A brief discussion is also given of projected performance based on techniques developed under this contract.

DESIGN

PERFORMANCE FACTORS

The sensitivity of a detector is commonly expressed in terms of its noise equivalent power (NEP), which is defined as the incident signal power, normalized to unit frequency bandwidth at a given operating frequency and radiation wavelength, for which the signal-to-noise ratio is unity. Another common measure of detector sensitivity is the detectivity (D*) given by

$$D^* = \frac{A^{1/2}}{NEP} = \frac{R_V A^{1/2}}{V_N} \qquad (1)$$

where

R_V = voltage responsivity

A = area of the detector element

V_N = voltage noise of the detector-preamp combination relative to the preamp output.

The NEP of a pyroelectric detector, including the preamplifier, can be written (ref. 8) as the quadrature sum of the contributions from the following noise sources:

1. Temperature noise
2. Intrinsic dielectric loss noise
3. Preamplifier current noise
4. Preamplifier voltage noise
5. Johnson noise of the load resistor.

To illustrate the relationship among the various noise sources, the NEP for a 2 μm-thick $LiTaO_3$ detector has been calculated (ref. 8) for parameters representative of our materials and preamps. The noise from the load resistor was not considered. Further, we assumed that the detector sensitive area was defined by metallized electrodes on a chip of $LiTaO_3$ material that was supported away from the sensitive area, as described in ref. 9. Since air conduction was not included, the thermal conductance G_T was due only to thermal diffusion within the $LiTaO_3$ material and radiative loss. Therefore, the NEP component due to temperature noise is given by (ref. 10)

$$NEP = \alpha^{-1} \, (4kT^2G_T)^{1/2} \tag{2}$$

where

α = detector absorptivity

T = detector temperature

k = Boltzman constant.

The detector absorptivity is taken to be unity for this analysis.

The results of this calculation are shown in Fig. 1. Note the importance of temperature noise where modulation frequency-detector area products are 1 to 20 mm^2 Hz, and the NEP is less than $3 \times 10^{-11} WHz^{-1/2}$. For a detector area = 1 mm^2 at 15 Hz, the NEP contribution from temperature noise exceeds that of any other noise source by more than 2.5 X. Moreover, if we consider the relationship of thickness (b) to NEP (ref. 8):

Temperature noise varies as $b^{1/2}$

Material loss tangent varies as $b^{1/2}$

Preamp current noise varies as b

Preamp voltage noise is independent of b

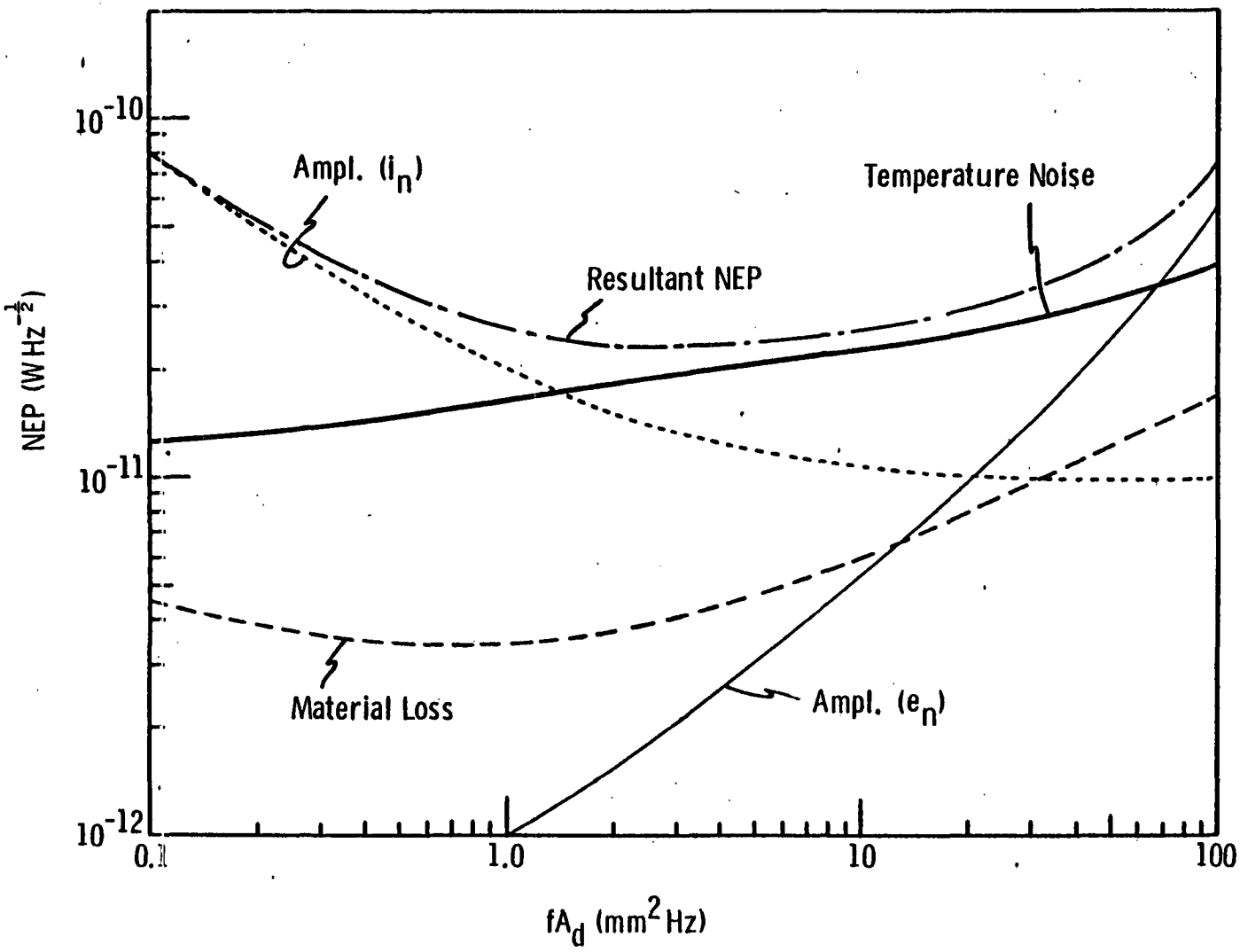

Fig. 1. Theoretical NEPs vs frequency-detector area product (fAd) due to various noise sources in a self-supported 2 μm-thick $LiTaO_3$ detector

Load resistor Johnson noise varies as b

temperature noise remains the dominant noise for b in the range 1-5 μm.

Therefore, a program to develop $LiTaO_3$ detectors with low NEP and high D* should consist of:

- Development of fabrication techniques for reducing the thickness of the detectors while lowering the thermal conductance between the sensitive detector area and its surroundings
- Development of a thin, highly absorptive coating for the IR region of interest
- Search for the lowest noise preamplifier available.

DETECTOR STRUCTURE

The detector designed for this contract was made from $LiTaO_3$ material in the so-called "bath tub-wagon wheel" construction (refs. 8, 9) (see Fig. 2). The sensitive area of the detector element was set at 1 mm^2, a value that allows good detectivity without unnecessary difficulties in manufacturing and measuring techniques.

The detector was designed for the minimum thickness that can be manufactured with a reasonable yield, i.e., thickness, b, = 1.5 μm. To handle such thin elements, it was necessary to design a thicker, i.e., stronger, edge around the sensitive detector area. As shown in Fig. 2, the 1-mm^2 sensitive area is defined by the overlapping area of the metallized coatings on the top and bottom of the detector element, and is surrounded by a thicker, non-sensitive edge. Lots of 16 detectors, containing eight detectors with an edge width of 30 μm and eight with an edge width of 60 μm, were processed on a single wafer (see "Detector Fabrication") simultaneously. The edge thickness was designed for a detector thickness of 3.5 μm. In addition to

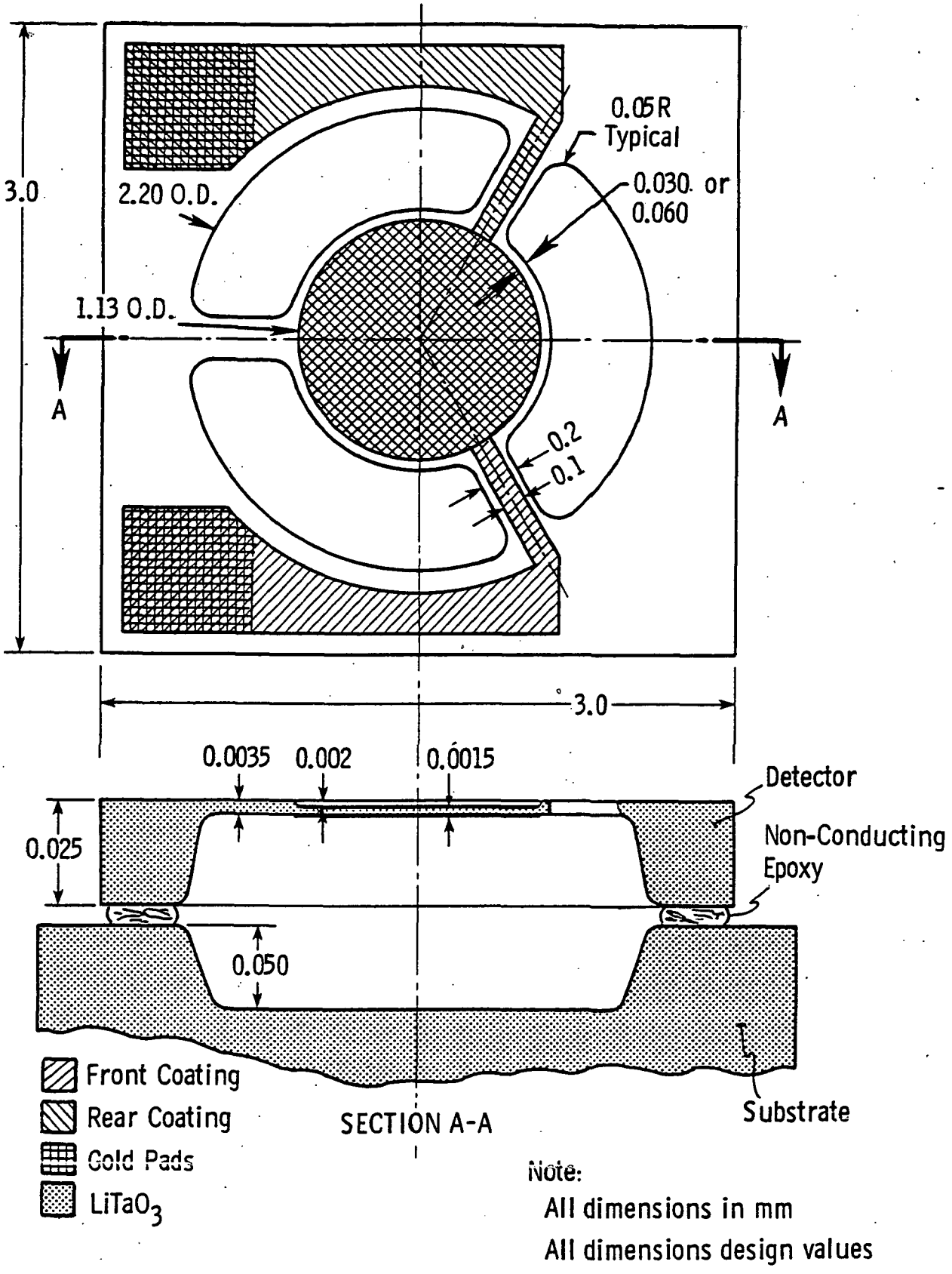

Fig. 2. Pyroelectric detector design

structural strength, the edge design imparted another advantage, namely, it increased the leakage path between the front and rear coating, thus minimizing surface conductance.

As discussed in "Performance Factors," to minimize temperature noise, it was important to reduce the heat losses due to conduction from the element to its supporting structure. This was done by using the reticulated "wagon wheel" construction shown in Fig. 2, in which the detector element (the hub of the wheel) was connected to the outer circumference by means of three support bridges (spokes of the wheel). The bridges were 2 μm thicker than the element, 200 μm wide, and approximately 500 μm long. Thus, at 15 Hz, the bridge length was over three thermal diffusion lengths (defined in "Dielectric Loss and Heat Transfer"), a satisfactory arrangement for reducing heat loss.

To strengthen the detector structure as much as possible without endangering any of the thermal-electrical characteristics, a "bath tub" construction was used. The outer wall of the bath tub, which was the supporting element, was 25 μm thick, and the inside (bridges and sensor element) was 3.5 μm or less. Consequently, it was possible to handle the detector structure with tweezers without damaging it. The thick outer wall had the additional advantage that it could withstand the mechanical and thermal stresses of wire bonding. For that reason, the conducting metallic thin films (front and back coatings) were connected by thin film leads across the bridges to gold pads on top of the outer wall of the bath tub.

As mentioned before, the sensitive areas of the detectors were covered with a metallic film on both sides of the $LiTaO_3$. These coatings were needed because the absorption of the pyroelectric material itself was not

sufficiently high over a wide spectral range. The design of these coatings is discussed in the next section.

The detector was mounted on a $LiTaO_3$ substrate so that thermal expansion coefficients would be the same, and the structural integrity of the wafer could be maintained at different temperatures. The detector-substrate bonding was done with epoxy.

The substrate was indented (see Fig. 2) to increase the distance between the sensitive element and the substrate so that, even in air or argon, the possible thermal conduction loss to the substrate was minimized.

In summary, our detector-substrate assembly design had the following beneficial features:

- The sensitive detector element was designed to the minimum, practical achievable thickness that would give the lowest noise figure.
- The reticulated wagon wheel construction minimized the thermal conductance through the support structure.
- The bath tub design stiffened the construction so that the risk of breakage during handling was reduced.
- The bonding pads were fully supported, permitting the use of reliable semiconductor bonding techniques such as thermal compression bonding.
- The lead-outs from the sensors were consistent with the need to maintain the sensors' thermal isolation.
- The interconnections between sensors and bonding pads were provided by metallizations on a common $LiTaO_3$ material supported by a substrate of the same expansion coefficient, thereby ensuring a more reliable interconnect.

ABSORPTIVE COATINGS

In general, the absorption coefficient of the pyroelectric material not sufficiently high over a wide spectral range, and, thus, absorptive coatings are required. Desirable characteristics for such coatings are high absorptivity, low heat capacity, and good thermal conductance to the pyroelectric material. Most suitable coatings are either black or metallic films.

Black coatings, such as lampblack or 3M Black Velvet Paint, permit the absorptivity of a pyroelectric detector to be increased over an extensive spectral range. The 3M Black Velvet Paint provides a flat spectral response and nearly 100% absorption between 400 nm and 40 μm (ref. 11). However, it is difficult to apply in the very thin layer necessary for maintaining high detector responsivity. Lampblack can be employed to provide absorption in the visible and near infrared, but it has very poor absorptivity in the 8-14 μm region. Blacks also have the disadvantage of poor adhesion to the substrate, and are difficult to apply in a high resolution pattern.

Thus, present detectors employ thin metallic films, such as nichrome, that serve as both electrodes and IR absorbers. In the 5- to 25-μm IR window, these films provide an average of 50% absorption (ref. 12) with the absorptivity limited mainly by reflection from the first metallic film.

Since absorption may be enhanced by the introduction of thin films which act as antireflection (AR) coatings, we developed a computer program (OPTAR) to calculate the absorptance, reflectance, and transmittance of such films on $LiTaO_3$. The program calculates these properties of the multilayer structure by the matrix method, wherein a complex matrix is created in terms of the Fresnel coefficients for each optical interface. The product of these

interface matrices is a resultant complex matrix descriptive of the entire multilayer structure from which reflectance, R, and transmittance, T, can be calculated. A development of the method is given in Heavens (ref. 13). The absorptance, α_c, is then calculated from the relation

$$\alpha_c = 1 - R - T \tag{3}$$

The response of the detector, however, depends not only on the coating absorptance, α_c, but also on the heat capacity of the coatings, H_c, relative to that of the detector element, H_D. Therefore, an effective absorptivity, α, which considers the effect of those coating factors on the responsivity is computed as

$$\alpha = \alpha_c H_D/(H_D + H_c) \tag{4}$$

The OPTAR analysis requires the complex indices of refraction and the thickness of the absorbing layers and $LiTaO_3$ as input. The indices of refraction of $LiTaO_3$ and the AR coating were calculated from known parameters and were found to be in agreement with results from reflectance and transmittance measurements. However, due to a lack of literature data on the parameters of nichrome films grown on $LiTaO_3$, a functional form of the index of refraction of nichrome had to be estimated from reflectance and transmittance measurements. This derivation, together with the OPTAR analysis program, was formulated prior to the commencement of this program.

OPTAR results indicated that a four-layer structure was best suited for the thin $LiTaO_3$ detector: a $LiTaO_3$ detection surface coated by nichrome on its parallel faces with an overlaying AR coating on the incident surface, i.e., AR coating/nichrome/$LiTaO_3$/nichrome, with the radiation incident on the AR coating. Analysis was performed at the start of this program to determine

the range of coating thicknesses which, when applied to the detector design of Fig. 2, maximized absorptance from 500 K black-body radiation. OPTAR analysis indicated that greater than 80% absorptance could be attained with the following coating design: AR coating, 0.15 $\pm$ 0.05 μm thick; nichrome coatings, 300 Å thick.

ELECTRONIC CIRCUITRY AND PACKAGING

The complete assembly consists of a detector subassembly mounted on a lithium tantalate substrate, which is then attached to a larger Al_2O_3 substrate with 1 mil gold wire and silver epoxy. This substrate also supports the load resistors and the FET transistors. The components are interconnected using thick film metallization and thermal compression wire bonding techniques as shown in Fig. 3. The resulting circuitry, shown in Fig. 4, is the electronic circuit commonly used as a preamplifier for pyroelectric detectors. The source follower configuration, as shown, allows the high detector impedance to be converted to a lower value that is compatible with conventional amplifiers. When the circuit has a high value load resistor (e.g., $10^{12}\Omega$), it provides the maximum detectivities at frequencies less than 1 kHz.

As an important component in the pyroelectric detection system, the JFET (junction-field effect transistor) must be selected for low gate leakage current and low noise voltage at low frequencies (1 to 20 Hz). Of the many JFET devices tested at Martin Marietta, device U-423, manufactured by Siliconex Incorporated, had the best performance characteristics -- I_G<0.2 pA, V_e(15 Hz) <20 nV/ Hz $^{1/2}$. The electronics substrate shown in Fig. 3 employs three JFETs, any of which can be selected during the final assembly stages.

The electronics substrate is epoxied to the header as illustrated in Fig. 5. The following measures minimize microphonic noise:

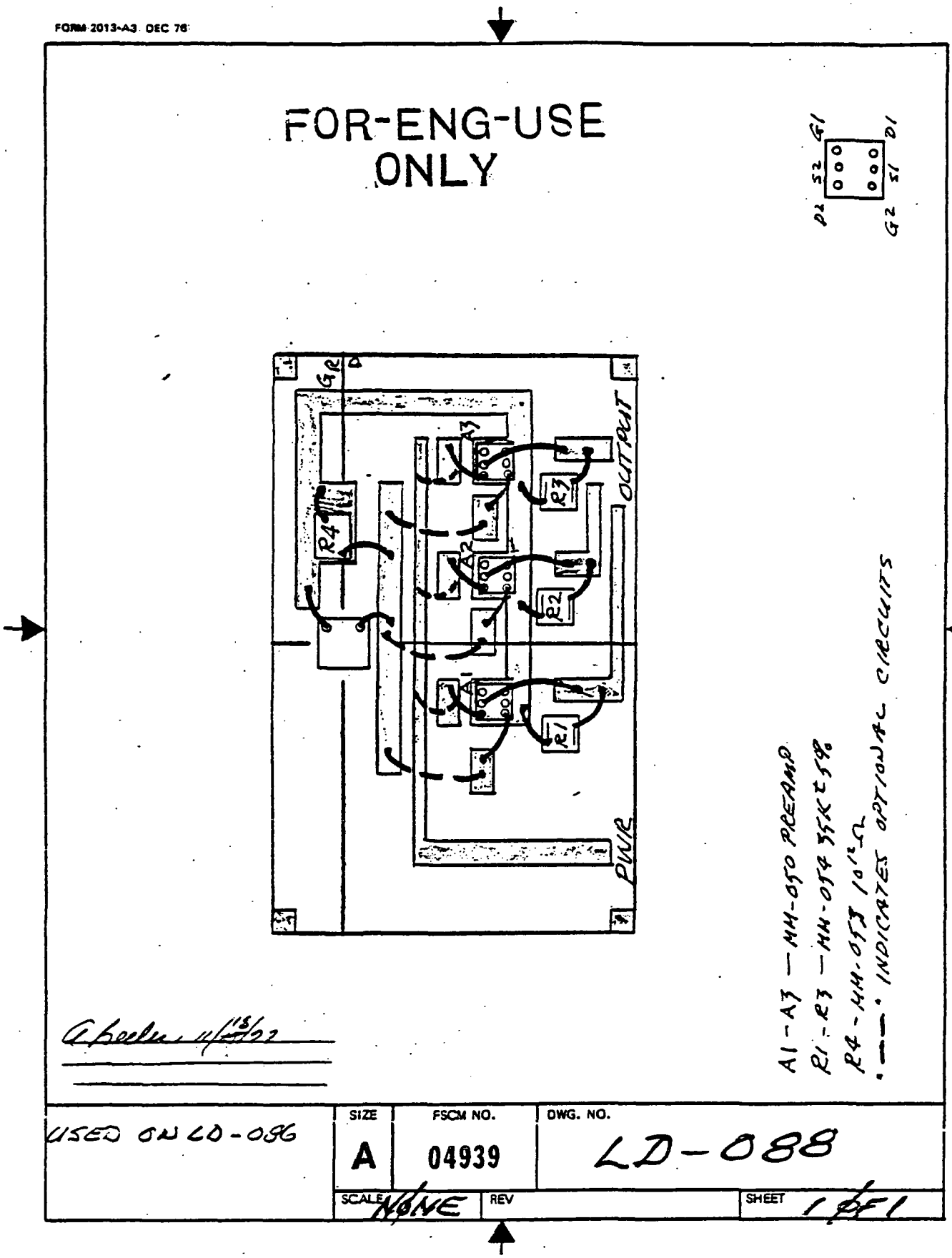

Fig. 3. Electronics substrate including JFETs, load resistors, and output resistors

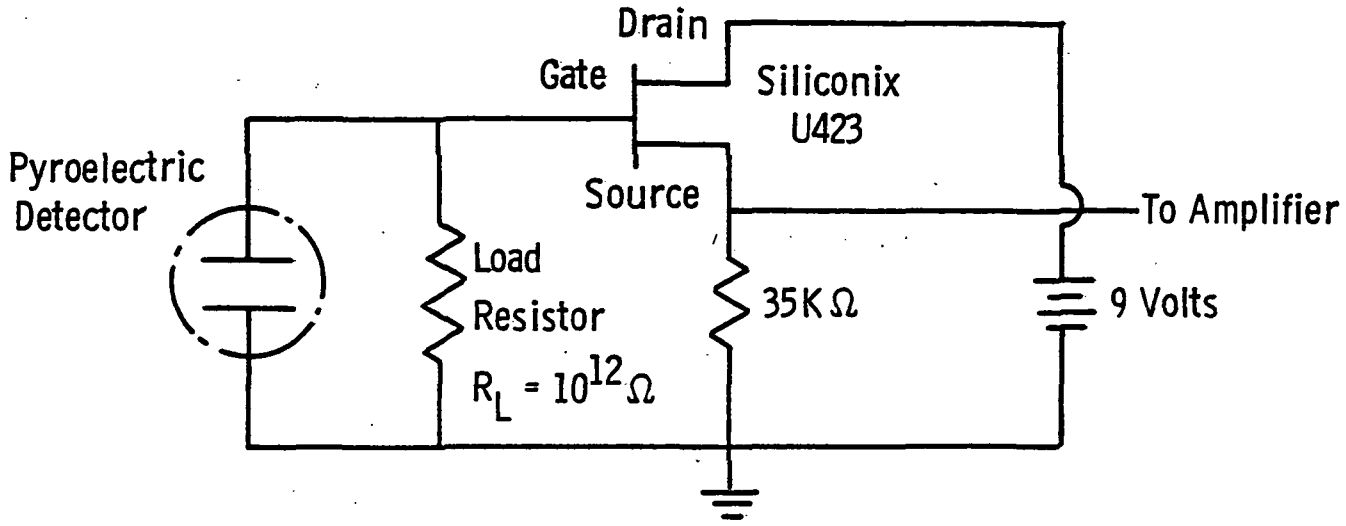

Fig. 4. Pyroelectric detector JFET preamplifier circuit

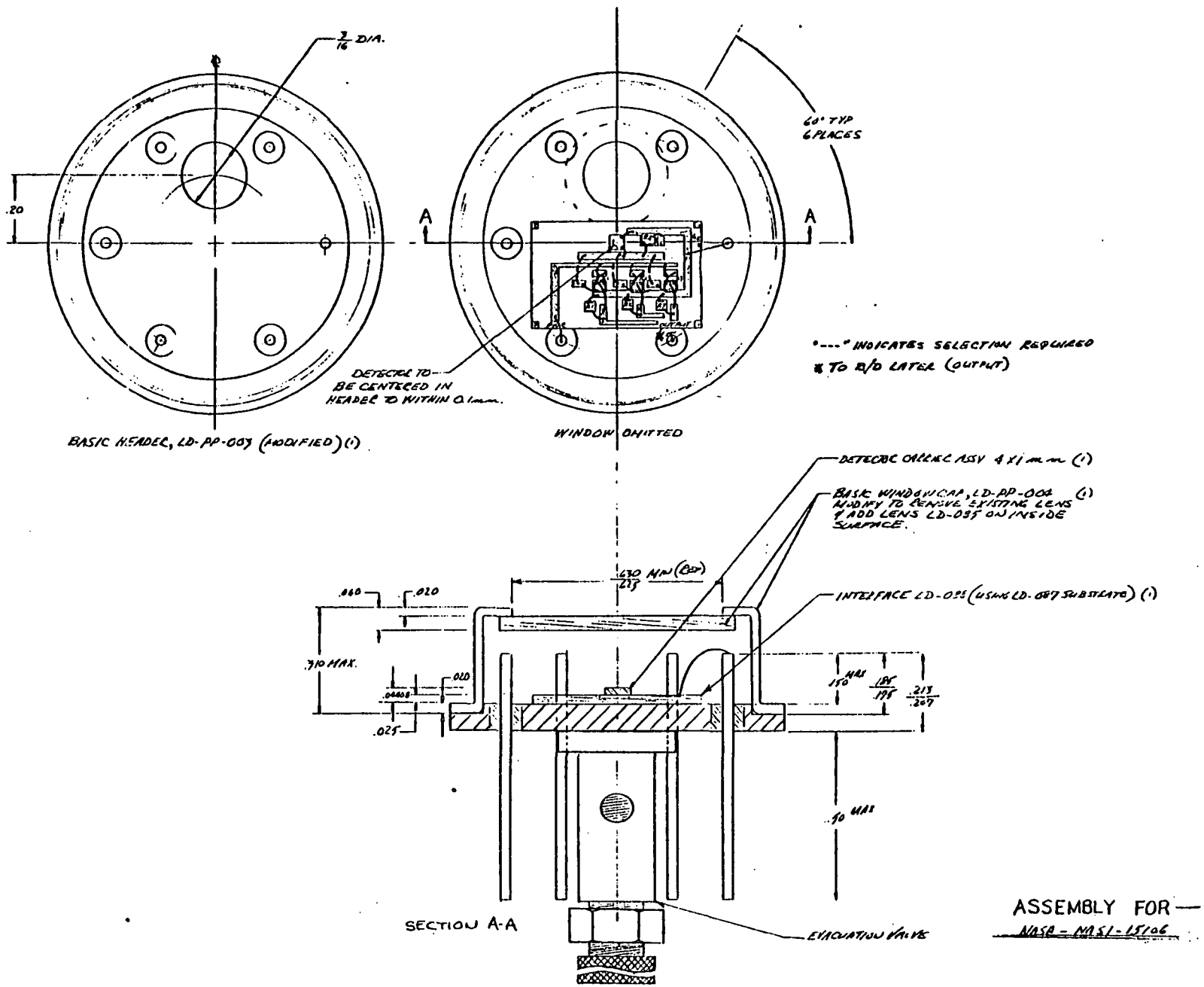

Figure 5. Detector assembly, including $LiTaO_3$ detector, preamplifier circuitry, header with evacuation valve, and germanium window

1. The lengths of wires interconnecting the detector, load resistor, and FET gate are kept to a minimum.
2. The high impedance circuitry is entirely contained on the electronics substrate.
3. The electronics substrate is rigidly attached to the header.

An evacuation valve is provided to permit the interchange of atmospheres within the header. The header cap, containing a 1-mm thick uncoated germanium window, is attached to the header with a low vapor pressure epoxy (torr seal).

FABRICATION

DETECTOR FABRICATION

The detector fabrication consists of the following important process steps:

1. Mechanical polishing
2. Photolithography
3. Ion beam milling
4. Assembly.

During our fabrication process, special care was taken to ensure that the specific material characteristics did not change, no deteriorating effects were produced, and the total loss due to handling was kept to a minimum. Nevertheless, in spite of these precautions, several wafers were damaged or lost because of the changes in the design. The combination of thin (<3 μm) detectors and AR coatings resulted in unforeseen difficulties which could not be solved within the limitations of this contract.

During all the process steps, the wafers, which consisted of 16 detectors each, were mounted on a holder. One of the first steps was the mechanical polishing of the first side of the wafer; the other side of the wafer was treated in the same way later.

It is common practice in the industry to use a slurry of silicon carbide for mechanical polishing. Naturally, the expertise of the operator and the proper usage of the equipment determine to a great extent the flatness of the polished surface and the degree of parallelism between the two sides of the

wafer. By using extreme care, we were, in general, able to keep the flatness less than 0.2 μm and the maximum deviation for flatness and parallelism combined less than 0.5 μm across the 1.5 cm-square wafer.

It is well known that mechanical polishing damages the crystalline structure of the material surface to a substantial depth and thus may cause an increase in the noise figure. However, it is possible to reduce the depth of this damage to less than 100 Å by removing the mechanically damaged layer by specially developed ion beam milling techniques (ref. 9). This rather new process for the production of clean, damage-free, pyroelectric detectors has been used extensively at Martin Marietta Laboratories and enables the manufacture of the bath tub-wagon wheel configuration designed for these detectors.

The same ion beam equipment can be used for sputtering metallic films onto the detectors. The advantage of this application is that an extremely good bond is produced between the film and the $LiTaO_3$ surface because the very high-energy sputtered metal particles penetrate deeply into the $LiTaO_3$ material. With this technique, it is possible to sputter gold directly onto a glass surface without an intermediate layer of chromium. Accordingly, the ion beam milling and sputtering processes were combined with photolithographic techniques to mill and sputter preferentially in certain areas of the wafers.

One of the major factors in producing good quality detectors is proper cleaning procedures. Where possible, the cleaning was done by ion beam techniques, especially in critical areas. When this procedure was not practical, e.g., when the cleaning had to be done prior to the mounting of the wafer on the substrate, chemical cleaning was sometimes used.

Work on the contract was initiated with the fabrication of four test wafers, identified as Z3, A4, B4, and R4. The main reason for the production of these wafers was to study the behavior of the different absorptive coatings.

Consequently, all the detectors that passed a visible inspection were mounted on a $LiTaO_3$ substrate, and nearly all detector-substrate assemblies were mounted on a TO5 header to facilitate testing procedures (see Table I). Every wafer contained 16 detectors, as mentioned before. By using special masking techniques, it was possible to produce four different coating tests per wafer (four detectors per test). Thicknesses of the AR coating were varied in these tests. The front coating consisted of nichrome approximately 300 Å thick covered with a 0.1 μm, 0.15 μm, 0.2 μm, or 0.25 μm-thick layer of AR coating. The back coating was also a nichrome film approximately 300 Å thick.

The manufacturing process of the wafers went rather smoothly without any major breakdown until the last process steps, namely, the stripping of the photoresist after the last sputtering step. During this procedure, the stripping fluid (or acetone) dissolves the glue in the slots of the wagon wheel construction and undercuts the glue that bonds the detector to the production holder. Consequently, removing the photoresist layer is a very delicate operation. In previous experiments on wafers thicker than 5 μm, the very different thermal expansion coefficients of the AR coating and the $LiTaO_3$ material had no deleterious effect on the wafers during photoresist removal. However, for this contract, the wafers were much thinner: the detectors located in the center part of the wafers Z3, A4, R4 had a thickness of 1.5 ± 0.4 μm, and that of wafer B4 was 2.6 ± 0.4 μm. As a result, trying to remove the photoresist was disastrous. All detectors acted as bi-metallic devices and curled very strongly at the edges. The strain created by this effect was sometimes so strong that the bridges for some wafers were torn loose. For that reason, it was impossible to clean the photoresist off properly, and nearly all the detectors of these

TABLE I. - WAFERS, DETECTORS, AND ASSEMBLIES FABRICATED UNDER CONTRACT WITH CORRESPONDING AR COATING THICKNESS*

Wafers	Detectors on TO5 Header	Detectors on Preamplifier	AR Coating Thickness (μm)
Z3			
A4	329		0.25
	342		0.10
B4			
R4			
H5	299		0.10
	300		0.25
	301		0.10
	302		0.15
	303		0.10
	304		0.25
I5			
J5			
K5	305		0.10
	306		0.10
	307		0.20
	308		0.25
	309		0.20
	310		0.25
	311		0.20
	312		0.20
	313		0.25
	314		0.10
M5		317	
	328		
	338		
	339		
	340	340	
	341		
T5		316	
	327		
	333		
	334		
	335		
	336		
	337		

*The nichrome coatings were 300 Å thick except for the detectors of wafer T5 where the front coating was 100-200 Å thick.

wafers were broken or gave unsatisfactory results (high electrical conductance). Detectors LT-329 and LT-342 of wafer A4 were the only ones mounted on a TO5 header.

The second group of wafers consisted of H5, I5, J5, and K5. During the fabrication process, wafer J5 was irreparably damaged because the ion beam milling equipment failed to run a constant ion beam current during overnight milling. For the same reason, wafer I5 had a wall thickness of 15 μm instead of 25 μm, which made it impossible to handle the detectors and to complete the final process steps.

Many detectors of wafers H5 and K5 were also irreparably damaged during the lifting of the photoresist in spite of a change in the process steps (gold was sputtered only on the thick outerwall of the detectors so that less cleaning of the thin surface was necessary). By reducing the amount of cleaning, it was possible to salvage approximately 50% of the detectors and to assemble them on to the substrate, but again, these improperly cleaned detectors had high electrical surface conductance, and some had poor connections. All the detectors had the tendency to curl at the edges, but the thicker detectors (approximately 2.3 $\pm$ 0.5 μm) curled far less than the others. At this time, we decided to use standard nichrome coatings only, so that we would not be hampered by the "curl" problem.

Wafers T5 and M5 were manufactured with front coatings of nichrome 100-200 Å and 250-350 Å thick, respectively. Thirteen detectors passed the visible inspection test. Since it was necessary to ship two detectors shortly to meet the contractual completion date, we screened for dielectric loss, and selected and mounted two detectors, LT-316 and LT-317, directly on the electronics substrate. The other 11 detectors were mounted on TO5 headers for further testing. The best detector of this lot, LT-340, was very

thoroughly cleaned before being mounted on the electronics substrate. The detector-preamplifier assembly was also cleaned again several times. Photographs of the assembly are shown in Fig. 6. Table I lists the detectors and wafers produced under this contract.

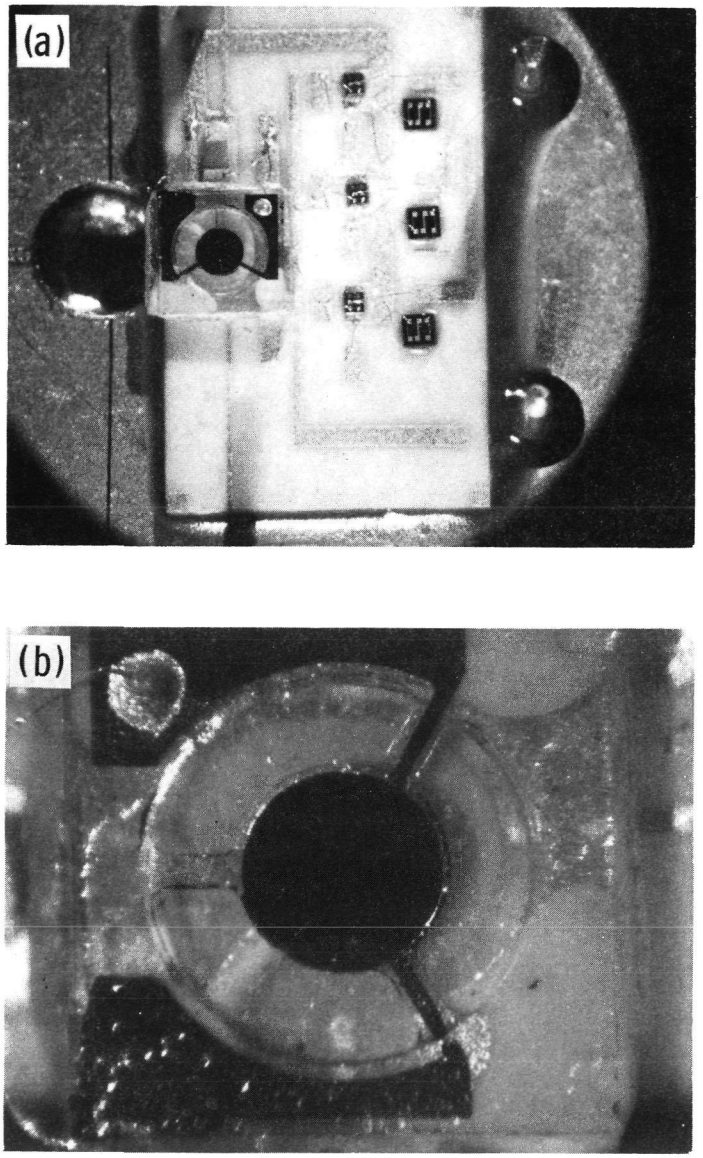

Figure 6. Photograph of (a) detector in header with associated preamplifier and (b) detector LT-340

TEST RESULTS

Test measurements and performance specifications were made for detectors fabricated from four wafers: A4, K5, M5, and T5. These wafers, which were selected for their low material loss tangents prior to processing, are characterized by the absorptive coatings listed in Table I. Chips delivered from these wafers were tested and selected for mounting onto TO5 headers for subsequent specification of loss tangent at atmosphere and in vacuum, and black-body and spectral response. Then, some detectors were poled and subjected to the procedures described below and retested. Details of absorptance and dielectric loss measurements are also provided below.

The detector-preamplifier assemblies were likewise tested for both air and vacuum operation (see "Preamplifier Characteristics"). Black-body response measurements with and without a germanium window, noise voltage measurements at ambient and 4°C, and vibration sensitivity measurements were made. These results are shown in "Detector-Preamplifier Assembly Characteristics."

DETECTOR CHARACTERISTICS

Absorptance values for 500 K black-body radiation are given in Table II for detectors designed and fabricated for this program. The absorptance, α, was derived from the voltage response R_V, by the relation:

$$R_V = g \frac{\alpha p}{\omega \rho c \varepsilon A} \cdot \frac{I(\omega)}{(1+C_s/C_d)} \qquad (5)$$

where

ω = the frequency and is large in comparison to the electrical time constant

TABLE II. - ABSORPTANCES α_{BB} DERIVED FROM THE RESPONSIVITY TO A 500 K BLACK-BODY RADIATION SOURCE OF DETECTORS MOUNTED ON TO5 HEADERS, WITH CORRESPONDING AR COATING THICKNESS AND WAFER ORIGIN

Detector	Wafer	AR Coating Thickness (μm)	α_{BB} (%)
LT-305	K5	0.1	46.2
LT-307	K5	0.2	59.4
LT-312	K5	0.2	59.8
LT-328	M5		49.6
LT-329	A4	0.29	60.9
LT-333	T5		51.3
LT-334	T5		52.6
LT-336	T5		53.2
LT-339	M5		53.0
LT-340	M5		53.8

g = gain of the FET follower preamplifier

p = pyroelectric coefficient

ϵ = dielectric constant

ρ = density

c = specific heat per unit mass

C_s = input capacitance of the FET circuit

C_d = capacitance of detector

$I(\omega)$ = factor containing the thermal response of the detector to a radiant input

A = area of the detector sensitive surface.

To insure that $I(\omega) \simeq 1$, only responsivity data at frequencies above 30 Hz were utilized. Absorptance spectra curves for LT-340, which had nichrome coatings only, and LT-329, which had an AR coating and nichrome coatings, are shown in Figures 7 and 8, respectively. A modest improvement in absorptance occurs when an AR coating is added, as can be seen in Table II. For example, the absorptance of LT-329 (AR-coated) is 16% greater than that of LT-339 (no AR coating). However, the best absorptance attained was significantly less than the value ($\alpha_{BB} > 80\%$) anticipated on the basis of the OPTAR analysis (see "Absorptive Coatings").

The major source of error in the OPTAR analysis is the uncertainty in the indices of refraction and thicknesses assumed for the nichrome films. Improved estimates of these parameters were obtained through more precise measurements of reflectance, transmission, and thickness of nichrome films sputtered on $LiTaO_3$ substrates. The complex indices of refraction of these films were then re-evaluated with OPTAR. The result was a 25% change in the calculated value of the index of refraction for the nichrome coatings. Using this new value, our OPTAR analysis program prescribed new multilayer structures with thicker AR coatings and thinner nichrome coatings. Because of time limitations, however, detectors could not be fabricated for this program

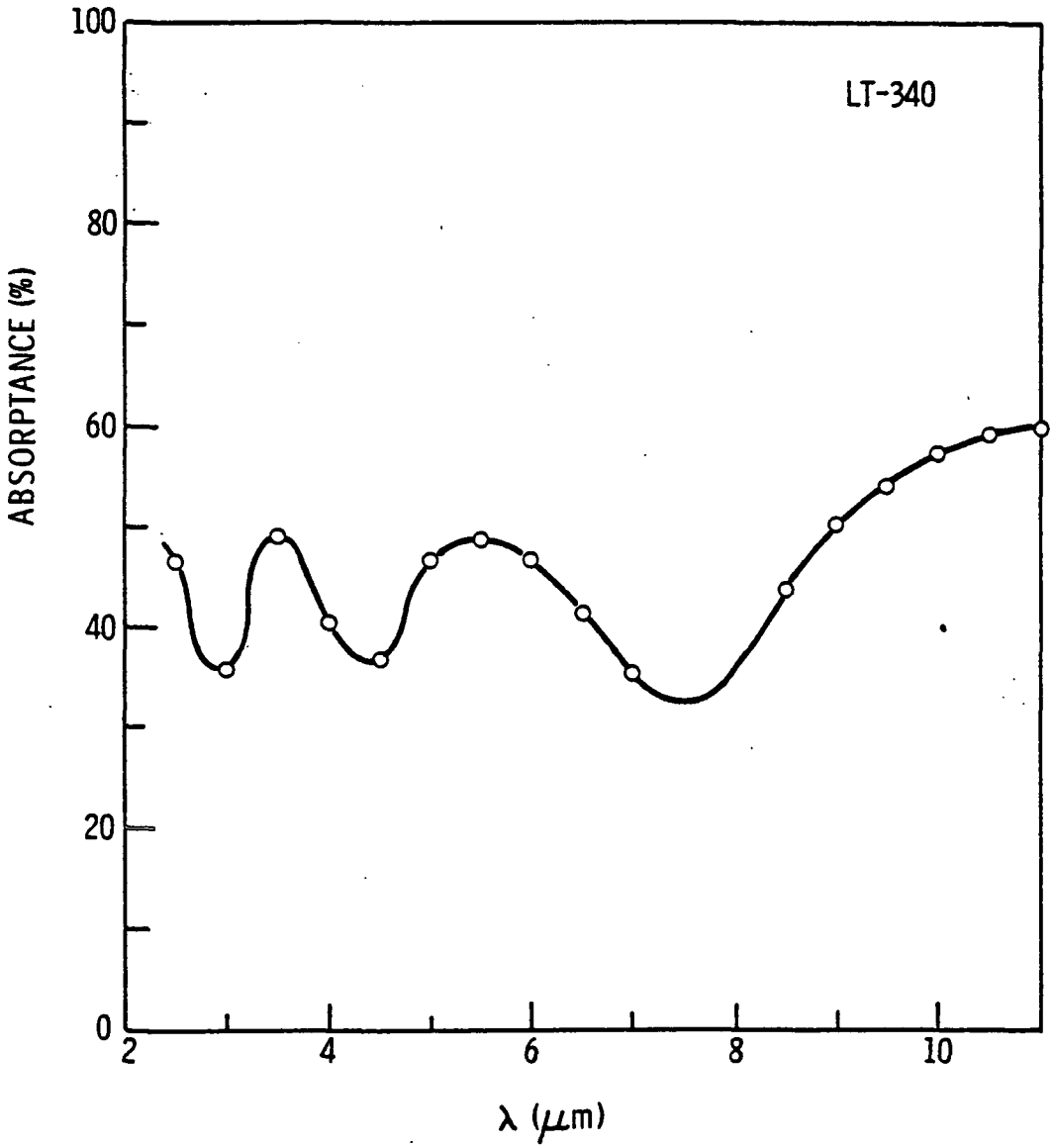

Fig. 7. Absorptance as a function of wavelength for detector LT-340

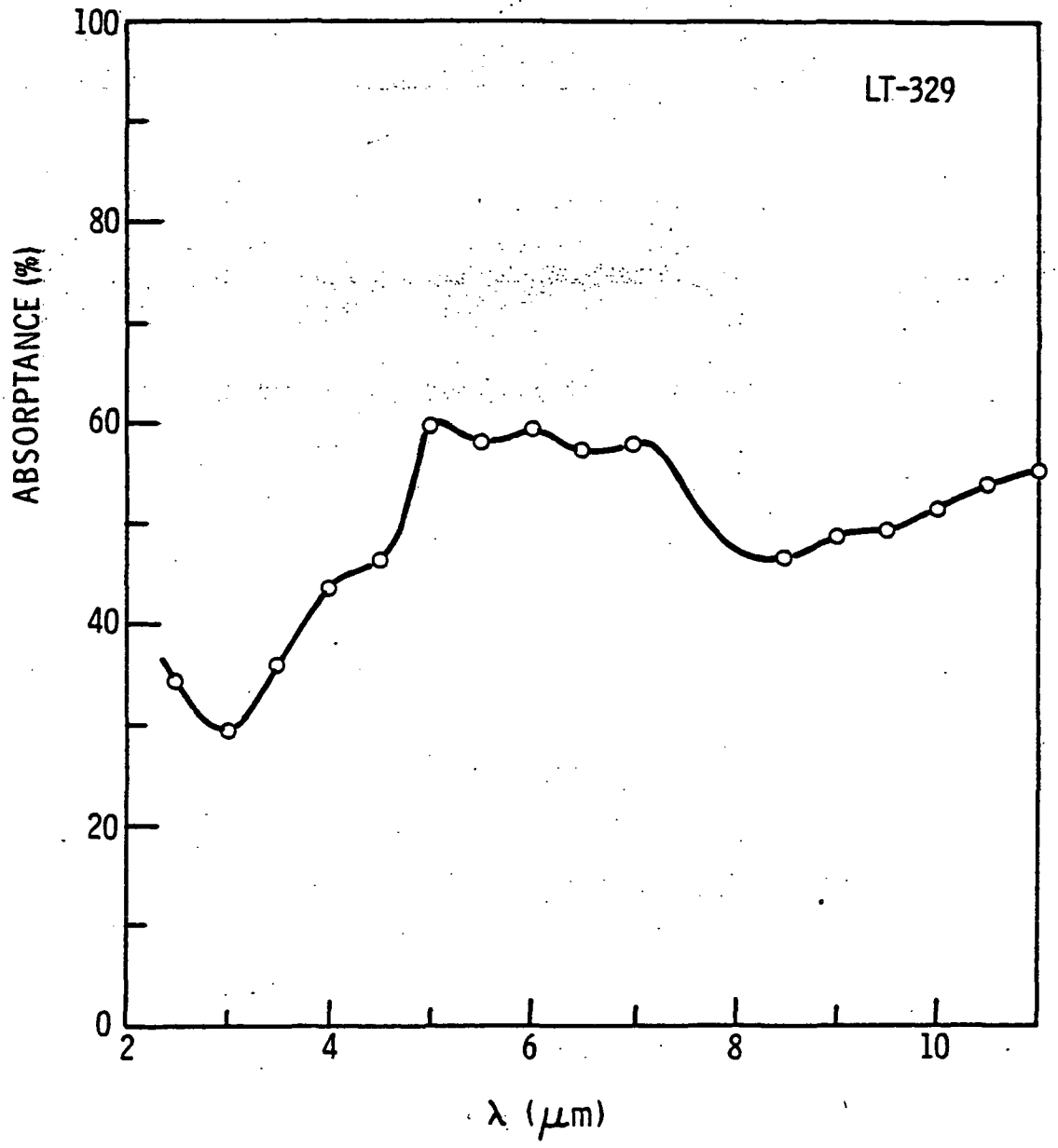

Fig. 8. Absorptivity spectrum for detector LT-329

with the prescribed coatings.

However, two detectors, LT-323 and LT-357 were designed based on the revised OPTAR results, and their absorptance spectra are shown in Fig. 9 together with the theoretical spectra. These detectors, which were designed for another program now in progress, were fabricated from separate wafers with 0.4-μm AR coatings. It can be seen that the actual spectra agree very well with the design. Black-body absorptances were calculated by weighing the absorptance spectra curves against a 500-K Planck distribution. The weighted absorptances were:

$$\text{LT-323:} \quad \alpha_{BB} = 77\%$$

$$\text{LT-357:} \quad \alpha_{BB} = 75\%.$$

Although these detectors were not designed for maximum 500 K black-body absorptance, a survey of OPTAR printouts over a range of coating thicknesses indicates that a coating set with significantly larger values of α_{BB} is unlikely.

The loss tangents, Δ, of the three detectors LT-316, LT-317, and LT-340 are shown in Table III for the detectors in air before mounting onto the preamplifier assemblies. In addition, the loss tangent as a function of frequency of LT-340 is shown in Fig. 10 for the detector on the TO5 header in a vacuum of approximately 50 mtorr. The dielectric loss is calculated from the capacitance C and conductance G by the relation

$$\Delta = \frac{G}{\omega C} \qquad (6)$$

Earlier, it had been found that milling processes in the fabrication of thin detectors (~2 or 3 μm) tended to depole them. Thus, a poling procedure was developed for thin, finished detectors which consisted of applying a field of 2×10^5 Vcm^{-1} at 70°C for about 20 minutes. These conditions were determined

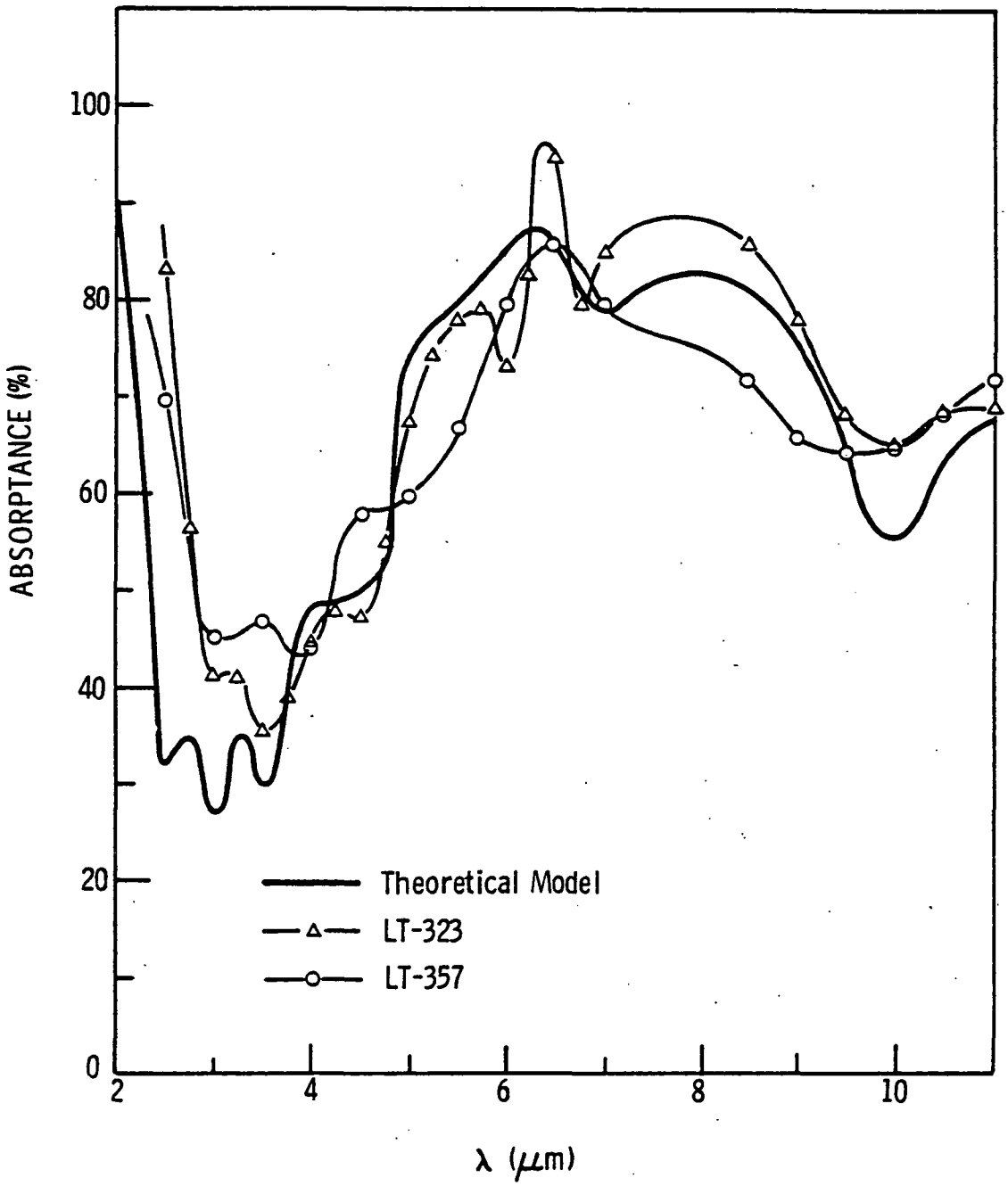

Fig. 9. Comparison of absorptivity spectra for detectors LT-323 and LT-357 with those derived from the OPTAR analysis. The units were fabricated under another program.

TABLE III. - CAPACITANCE, CONDUCTANCE, AND DIELECTRIC LOSS OF DETECTORS AT 15 Hz ON TO5 HEADERS, AND VARIATION OF THESE PARAMETERS WITH POLING AND ATMOSPHERIC PRESSURE FOR DETECTOR LT-340

(Thickness is derived from capacitance measurement.)

Detector	Capacitance, C (pF)	Conductance, G (pS)	Dielectric Loss, Δ (10^{-3})	Thickness, b (μm)
A. In air at atmospheric pressure:				
LT-316	121.47	63.0	5.50	3.1
LT-317	115.09	42.6	3.90	3.3
LT-340	174.30	80.1	4.88	2.2
B. In vacuum (45 mtorr) before poling:				
LT-340	173.496	51.75	3.16	
C. In vacuum after poling:				
LT-340	172.404	32.9	2.02	
D. At atmospheric pressure (air) after poling:				
LT-340	173.07	70.0	4.29	

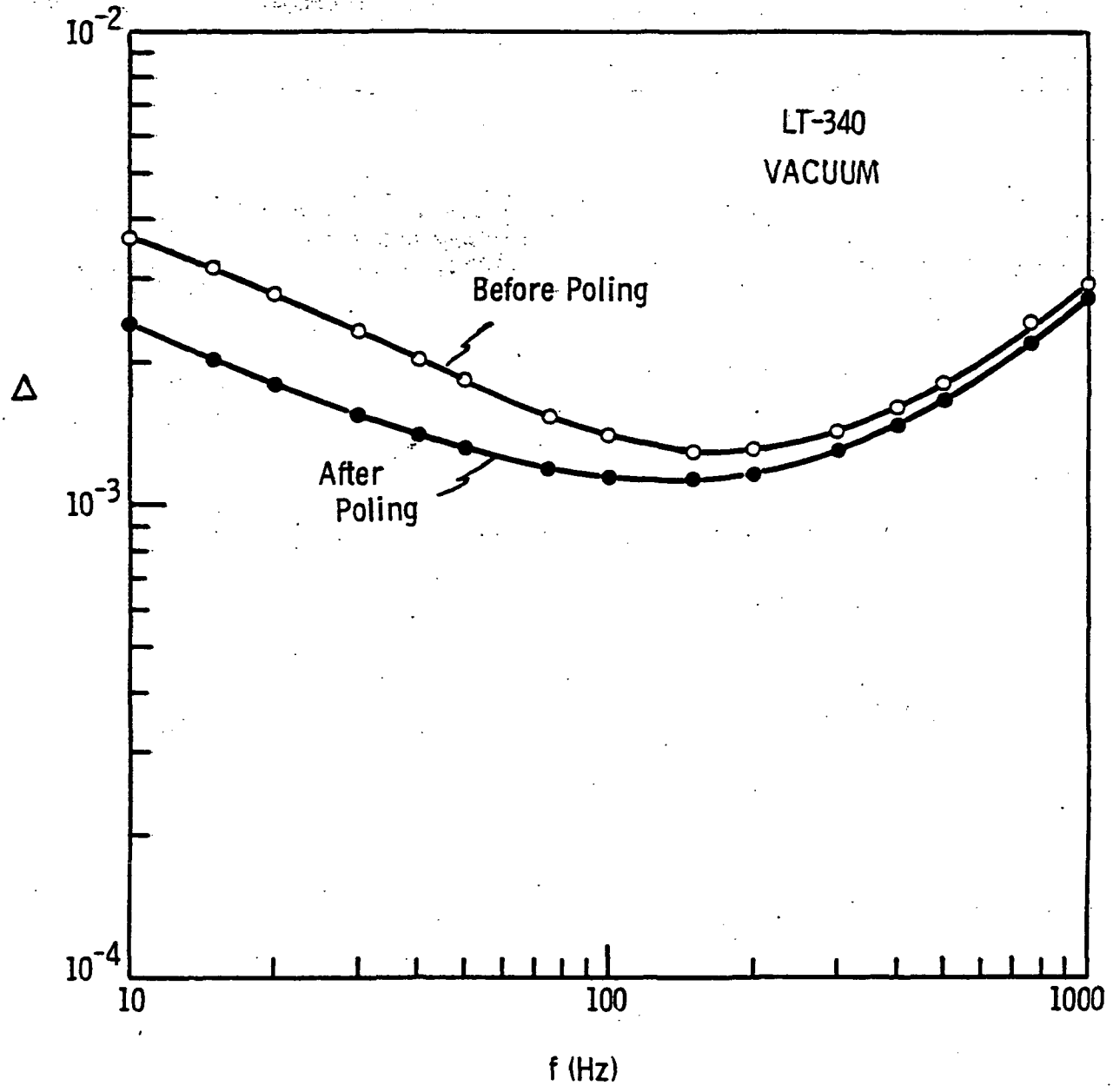

Fig. 10. Detector LT-340 loss tangent, Δ, at 50 mtorr pressure before and after electrical poling

after much experimentation and have always yielded good results.

It is seen in Fig. 10 that Δ in vacuum for detector LT-340 is improved by 36% as a result of poling, while Table III shows that poling and vacuum operation result in a 59% improvement. Note that, unlike LT-340, LT-316 and LT-317 were not poled or subjected to a final cleansing rinse. We would expect their losses to show similar reductions had these processing operations occurred.

In Fig. 11, the Δ for LT-340 in vacuum is separated into three components: 1) a material loss of 2×10^{-4}, measured for the wafers prior to fabrication; 2) a series resistance loss corresponding to a series resistance of 2100 Ω, which arises primarily from the leadouts; and 3) a residual loss, which is the most significant component at low frequency.

PREAMPLIFIER CHARACTERISTICS

The preamplifiers were characterized prior to final assembly. A gain of 0.866 was measured for preamplifier #4 and is consistent with previous measurements made for other Siliconix U-423 FETs in identical circuits over the frequency range of 10 Hz to 1000 Hz (Fig. 4). Noise voltage measurements at the outputs gave values of approximately 9 $nV/Hz^{1/2}$ at 1000 Hz for the devices at atmospheric pressure. From the data for LT-340 (see "Noise" in "Discussion"), a best fit output noise voltage of 7.7 $nV/Hz^{1/2}$ was deduced for the devices under vacuum. The gate leakage current I_{Gss} for the three preamplifiers used was approximately 0.1 pA. Values for each preamplifier assembly, measured with a supply voltage of 10 volts, are given in Table IV with the manufacturer's specifications for the U-423 FET.

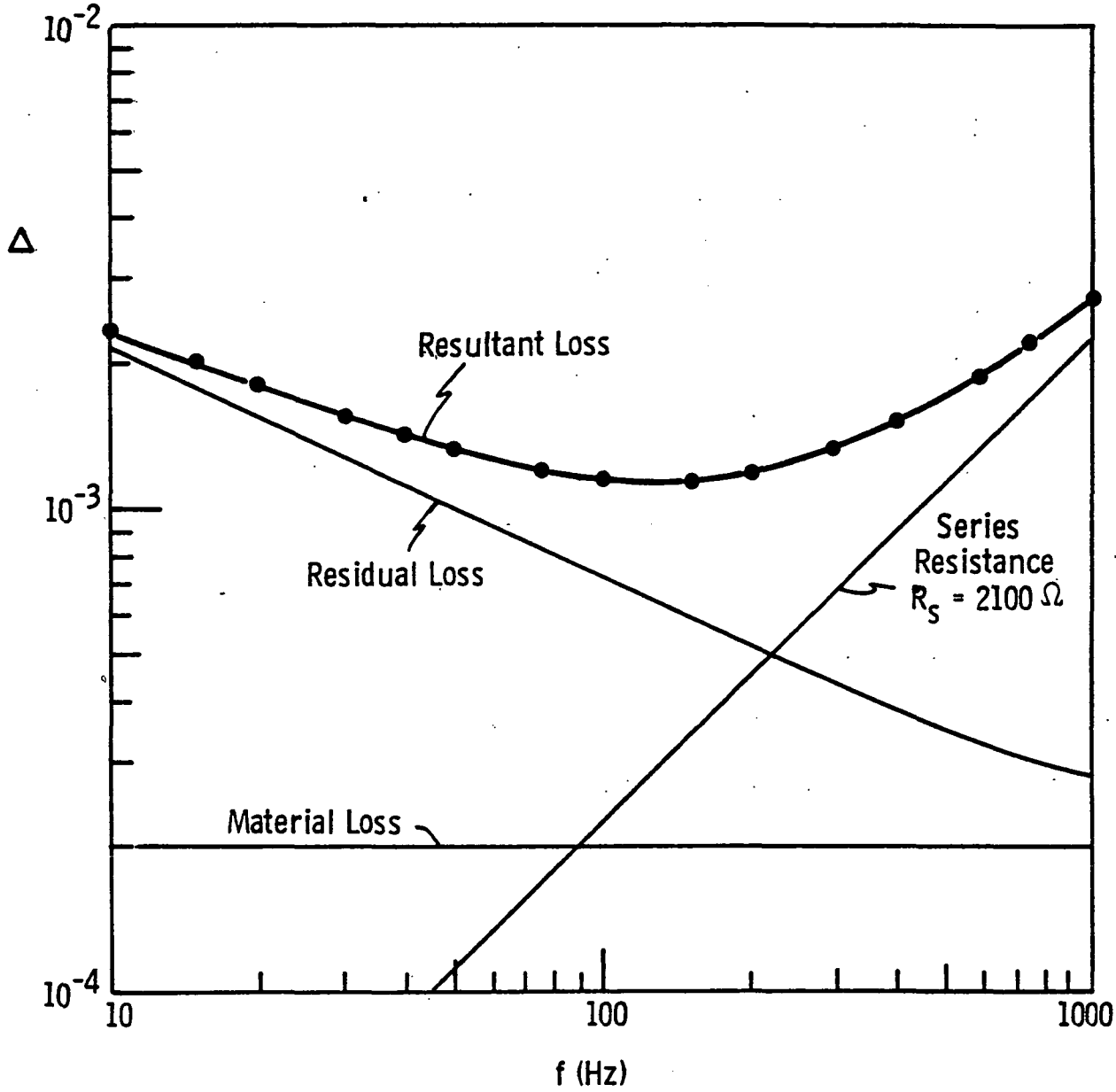

Fig. 11. Separation of the Δ of Fig. 10 (after poling) into a material loss, a series resistance loss (R = 2100 Ω), and a residual loss

TABLE IV. - GATE LEAKAGE CURRENT AND NOISE VOLTAGE AT 1000 Hz FOR PREAMPLIFIERS 1, 4, AND 5, TOGETHER WITH THE SPECIFICATION BY SILICONIX FOR THE U-423 JFET (Voltage source is 10 volts.)

Preamplifier	Associated Detector	Gate Leakage Current, I_{Gss} (pA)	Noise Voltage, V_e ($nV/Hz^{1/2}$)
1	LT-316	0.075	9
4	LT-340	0.110	9
5	LT-317	0.120	9
Mfg. specs.		0.050	10

DETECTOR-PREAMPLIFIER ASSEMBLY CHARACTERISTICS

For the detector-preamplifier assembly, the responsivity is given as a function of chopping frequency for an unfocused 500 K black-body source. Figures 12-17 show the assembly results for the detectors at atmospheric pressure and in vacuum (40 mtorr). Data presented are adjusted to be equivalent to those obtained for a window of 100% transmission. The actual window transmission was determined to be 50%, based on 500 K black-body response measurements for the detector LT-317 with and without the germanium window. The 50% transmission was later verified by measuring the 500 K black-body output power with and without the germanium window with a flat spectral response radiometer.

Comparison of the data for the three assemblies in Table V reveals that LT-340 has the lowest responsivity. This is attributed to its relatively low absorptance with respect to 500 K black-body radiation (see Table II). LT-316 has the highest responsivity, 836.2 V/W. Unfortunately, it, as well as LT-317, was not poled. Poling could be expected to improve the responsivities.

The noise voltages measured at the preamplifier outputs for LT-316, LT-317, and LT-340 are given in Table V for the assemblies under vacuum. Noise spectra for the assemblies are shown in Fig. 18. As expected on the basis of dielectric loss data, LT-340 has the lowest output noise voltage.

Cooling the LT-340 assembly to 4°C produced no measurable difference in output noise voltage.

D*, which is given by eq. (1), is shown in Fig. 19 and in Table V. A D* of 1.34×10^9 $cmHz^{1/2}W^{-1}$ has been achieved for LT-340 at 15 Hz.

Vibration sensitivity, R_{vib}, of the assemblies was measured at an acceleration of 1 g (9.8 m/s^2), and values for the three assemblies are given in

Table V at several frequencies. These results are comparable to those obtained for unreticulated detectors of the same area (typically 30 μV/G) (ref. 6). Further reductions in R_{vib} can be achieved using the complementary structure (ref. 14).

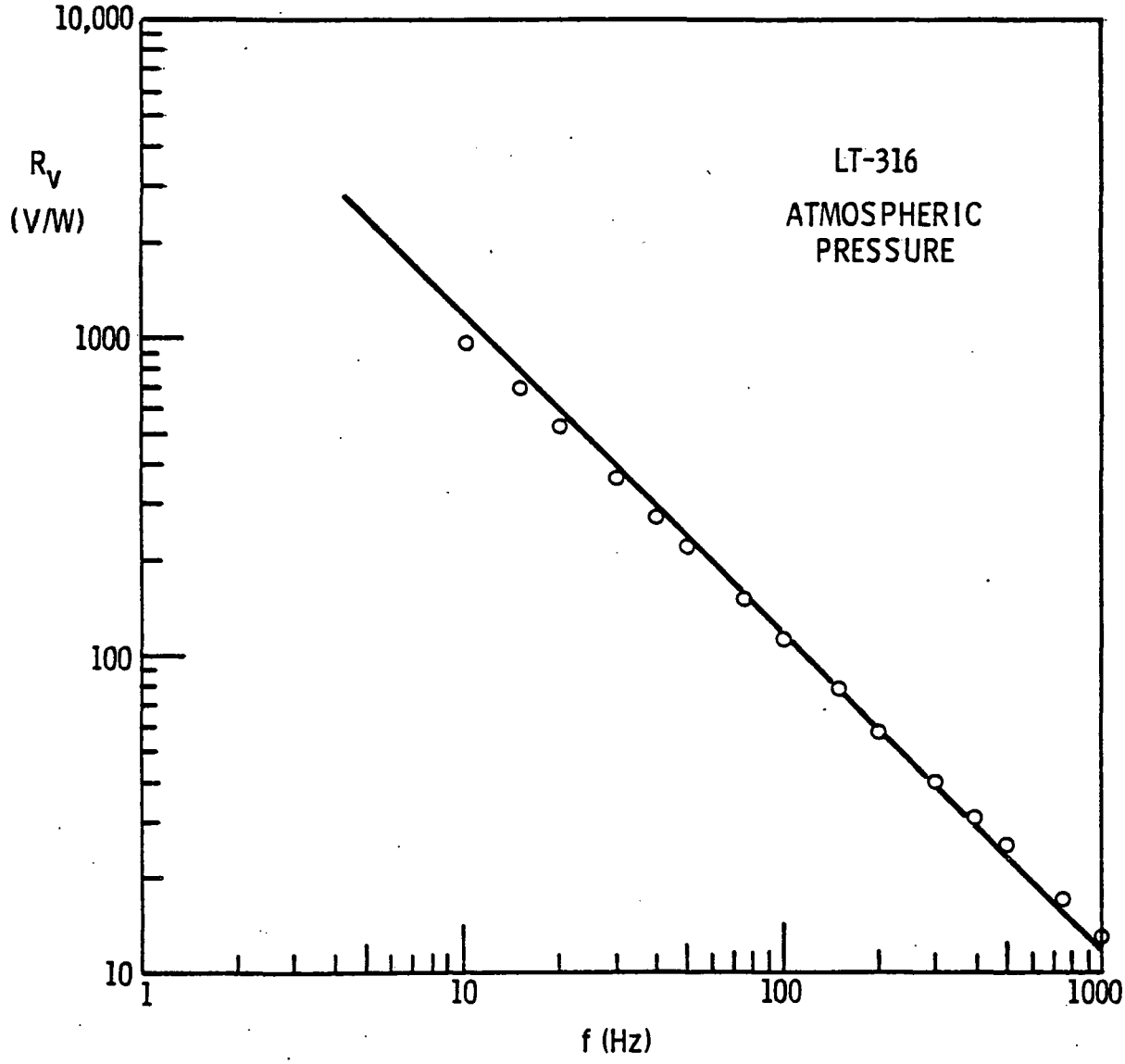

Fig. 12. Responsivity of the LT-316 assembly in air as a function of modulation frequency for a 500 K black-body radiation source

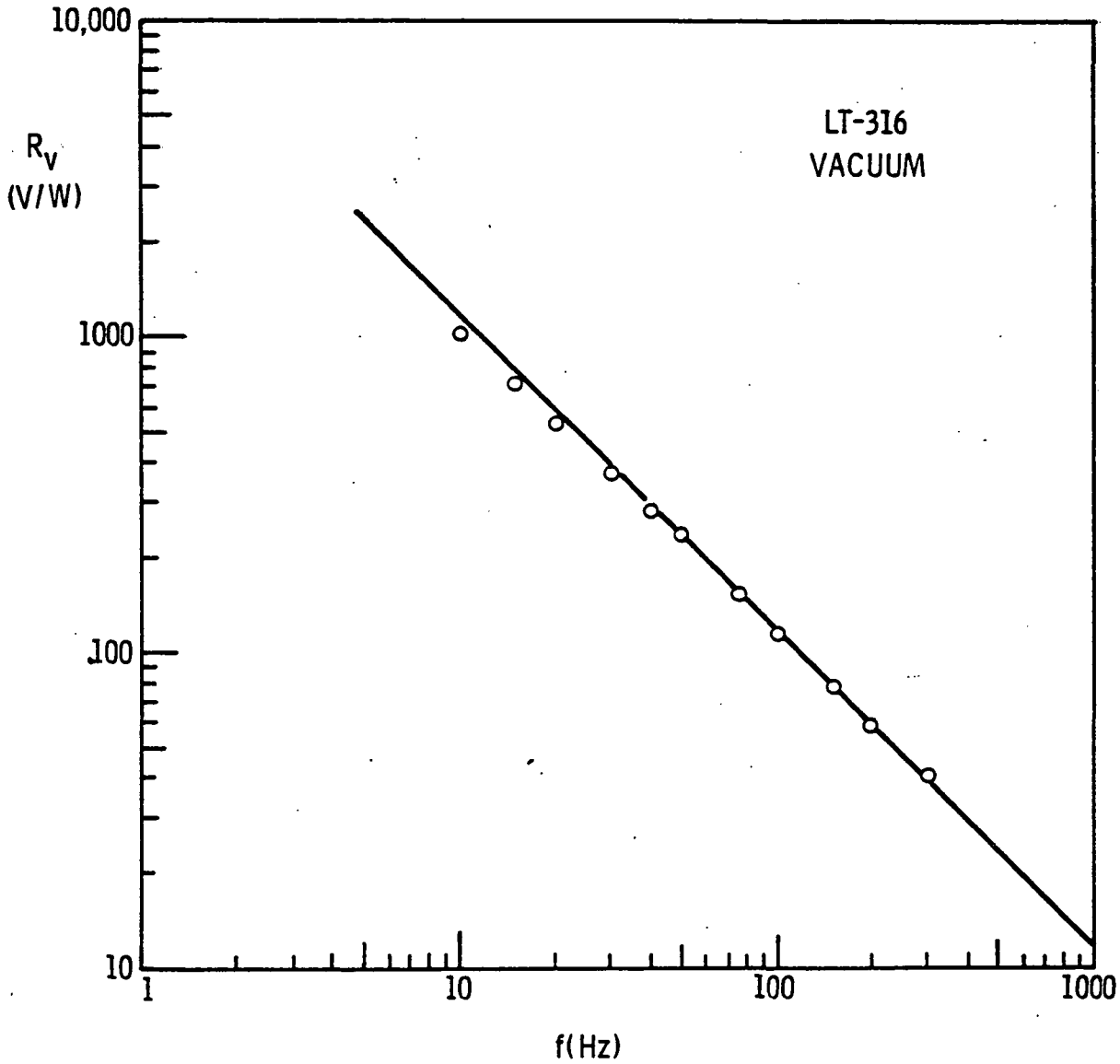

Fig. 13. Responsivity of the LT-316 assembly in 40 mtorr vacuum as a function of modulation frequency for a 500 K black-body radiation source

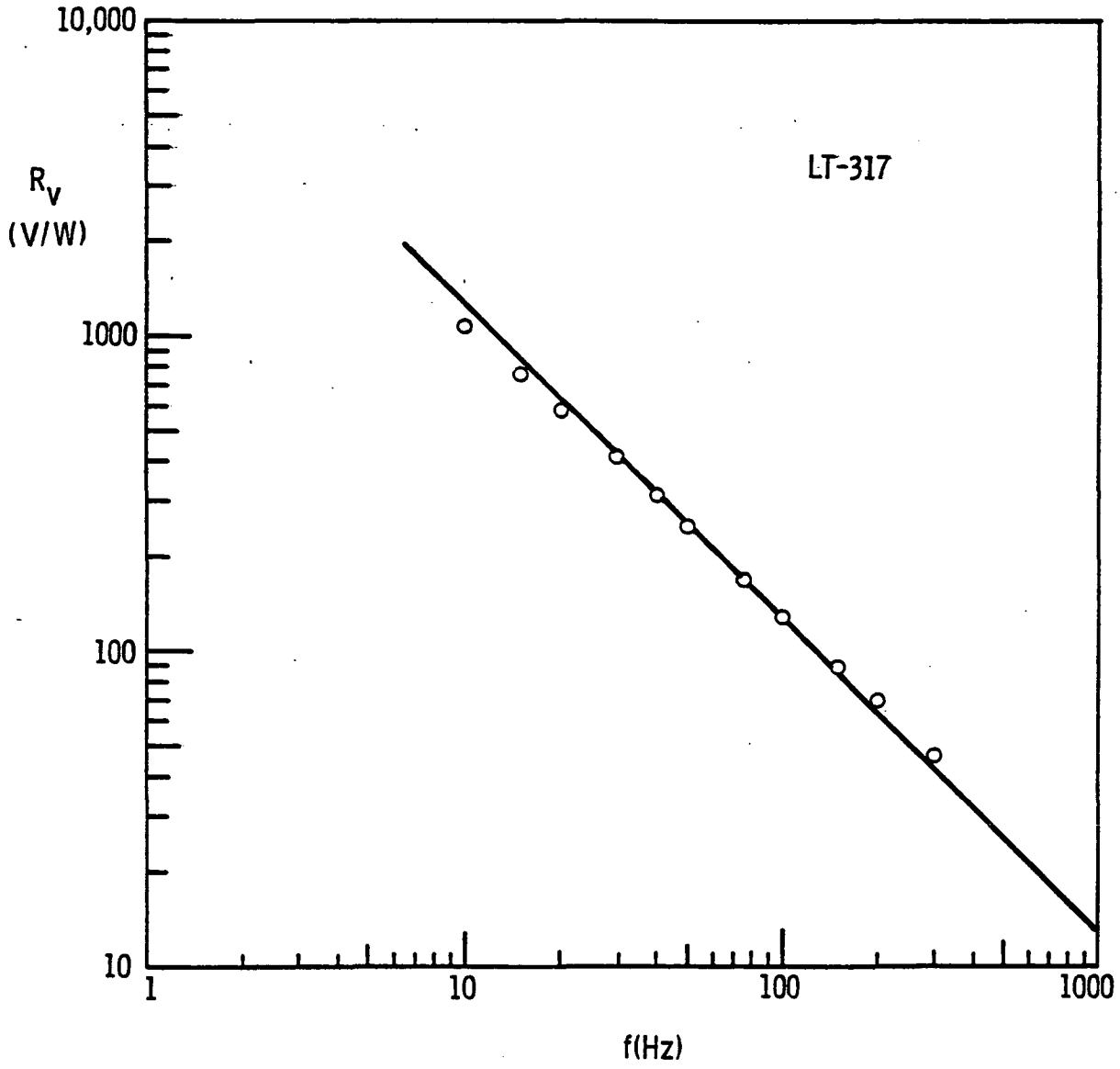

Fig. 14. Responsivity of the LT-317 assembly in air as a function of modulation frequency for a 500 K black-body radiation source

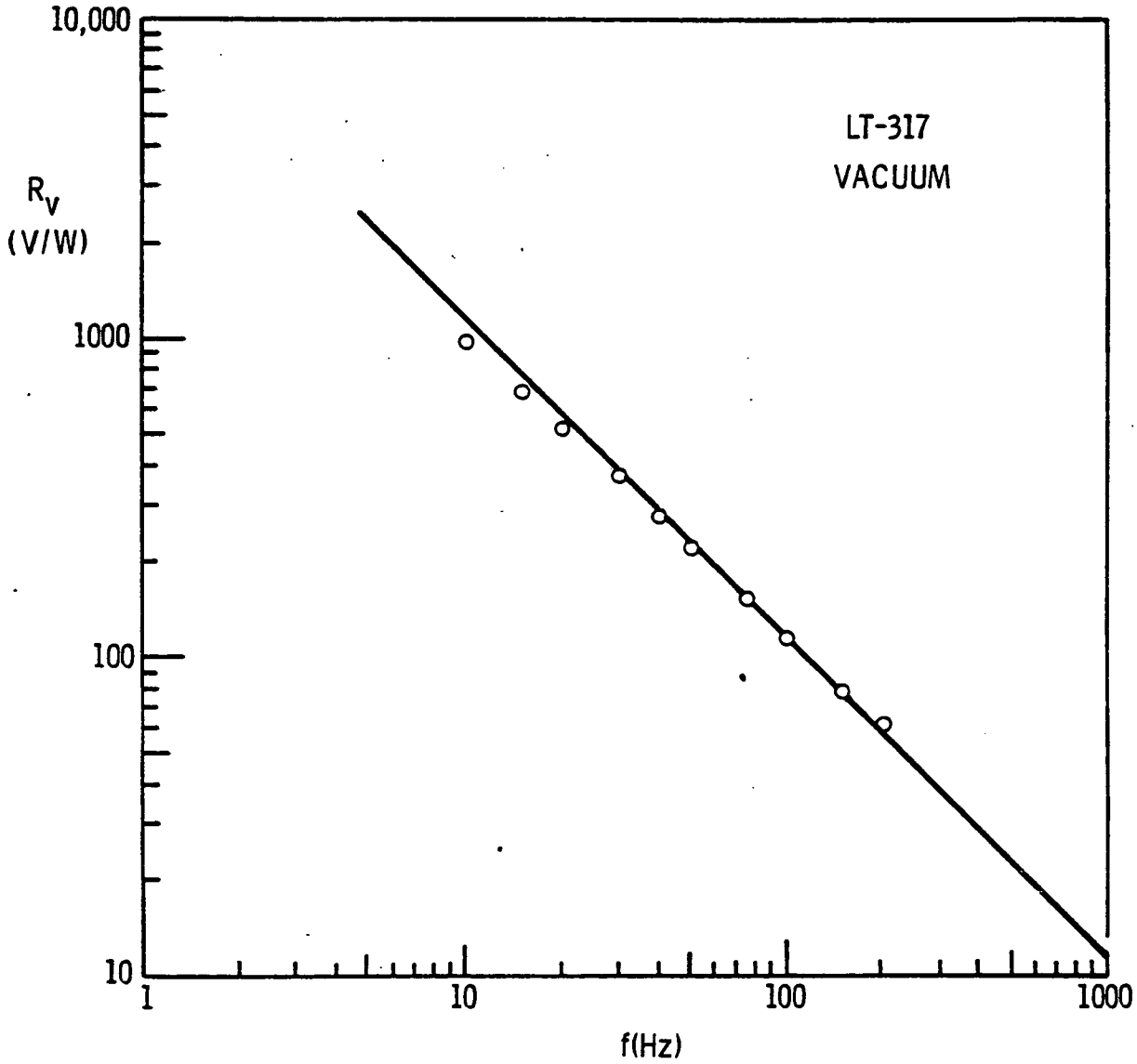

Fig. 15. Responsivity of the LT-317 assembly in 40 mtorr vacuum as a function of modulation frequency for a 500 K black-body radiation source

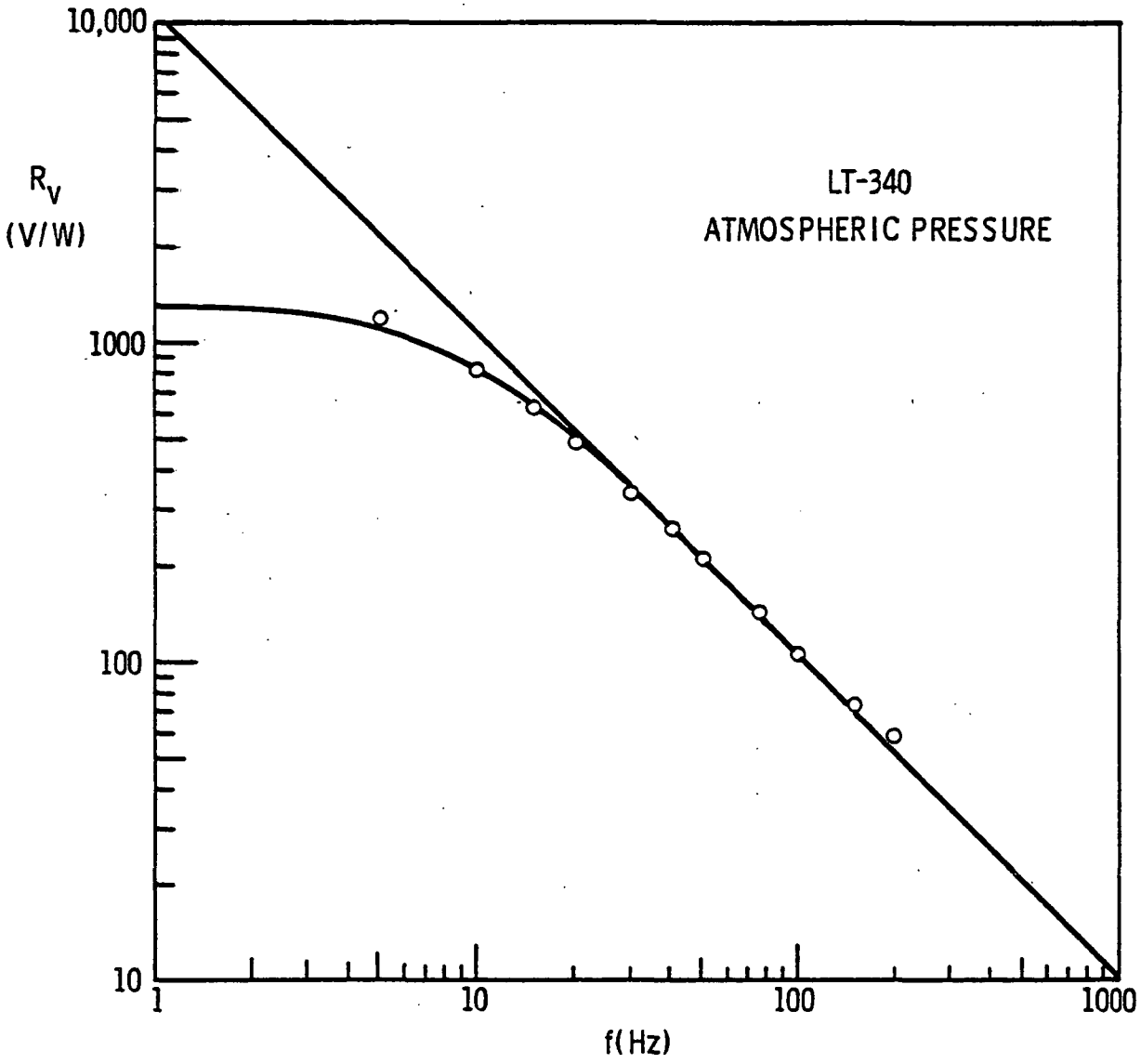

Fig. 16. Responsivity of the LT-340 assembly in air as a function of modulation frequency for a 500 K black-body radiation source

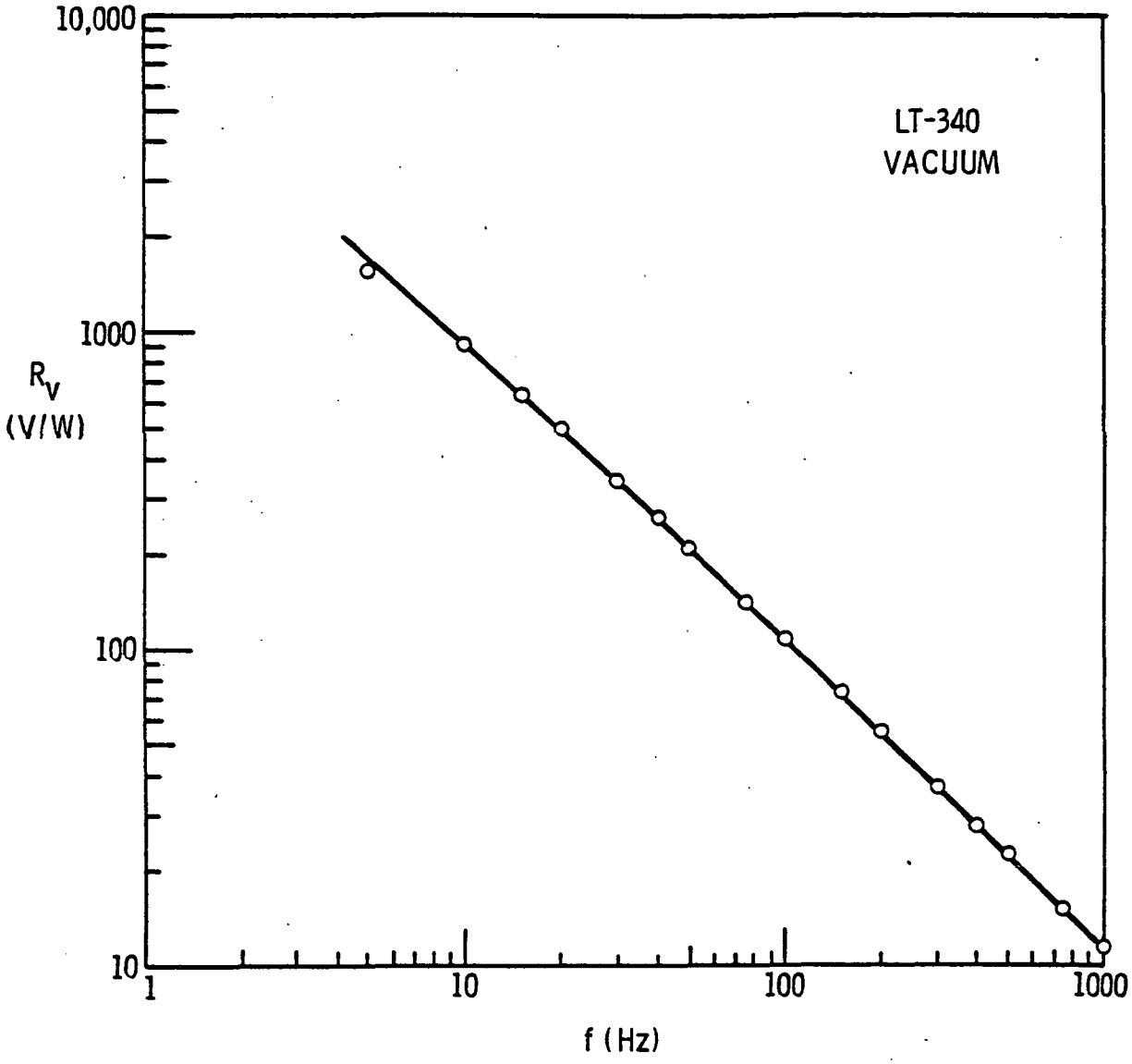

Fig. 17. Responsivity of the LT-340 assembly in 40 mtorr vacuum as a function of modulation frequency for a 500 K black-body radiation source

TABLE V. - NOISE VOLTAGE, RESPONSIVITY, DETECTIVITY, ABSORPTANCE, AND VIBRATIONAL SENSITIVITY FOR DETECTOR/PREAMPLIFIER ASSEMBLIES LT-316, LT-317, and LT-340 AT VARIOUS FREQUENCIES (All measurements made with assemblies under pressure of 45 mtorr.)

	LT-316	LT-317	LT-340
Noise Voltage, V_n ($nV/Hz^{1/2}$)			
10 Hz	90-100		65
15 Hz	70-100	65	48
100 Hz	19	30	19
1000 Hz	12	12	9
Responsivity, R_V (V/W)			
15 Hz	721.9	690.2	642.1
100 Hz	114.3	115.2	108.0
1000 Hz		12.3	11.2
Detectivity, D* ($10^9 cmHz^{1/2}W^{-1}$)			
15 Hz	0.85	1.06	1.34
100 Hz	0.60	0.38	0.72
1000 Hz		0.10	0.12
Absorptance, α_{BB} (%)	58.8	59.3	55.6
Vibrational Sensitivity, R_{vib} (V/g)			
15 Hz			60×10^{-6}
100 Hz	21.5×10^{-6}	52×10^{-6}	54×10^{-6}

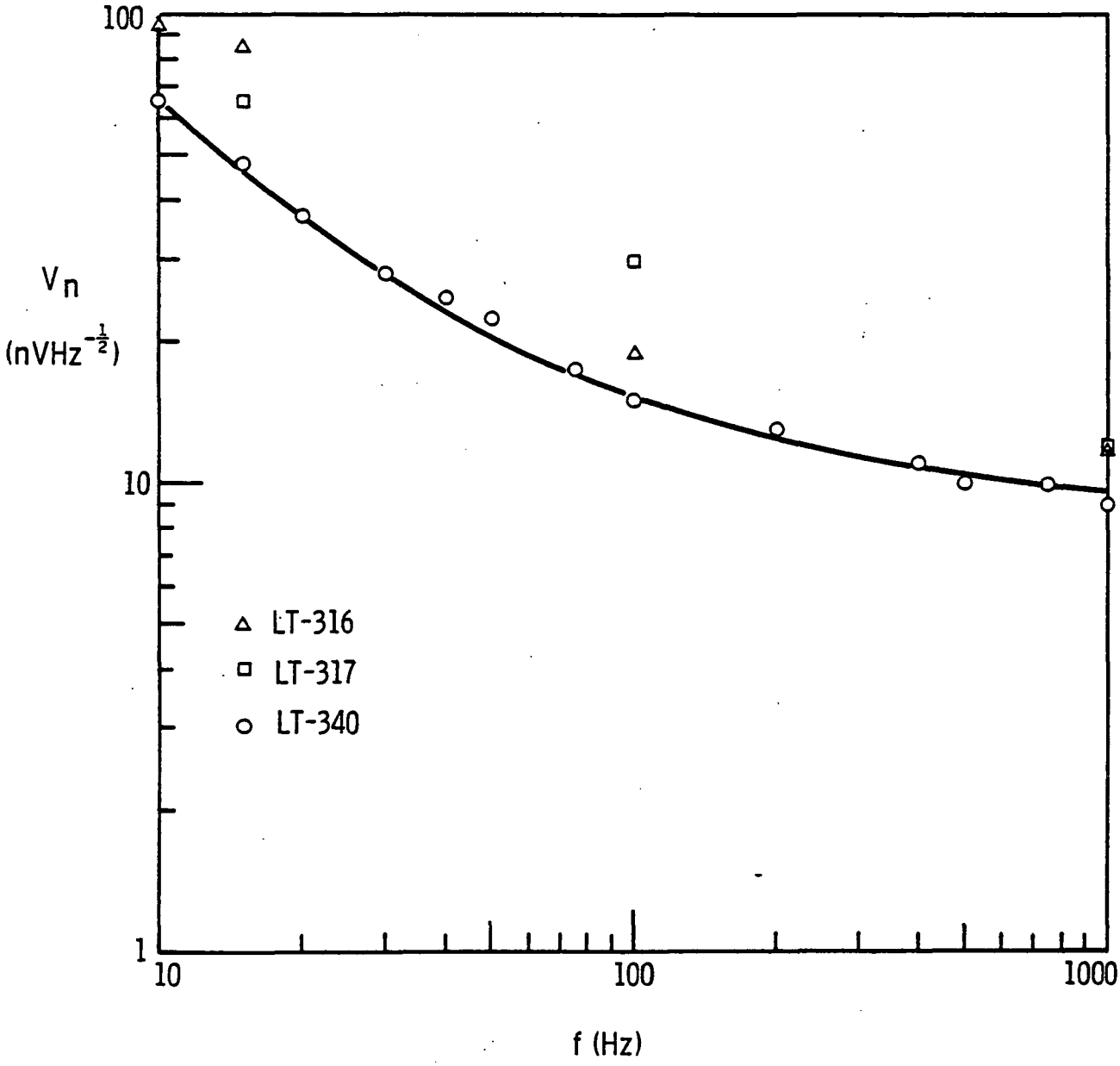

Fig. 18. Noise voltages for LT-316, LT-317, and LT-340 assemblies as a function of frequency for detector-preamplifier assembly under 40 mtorr pressure.

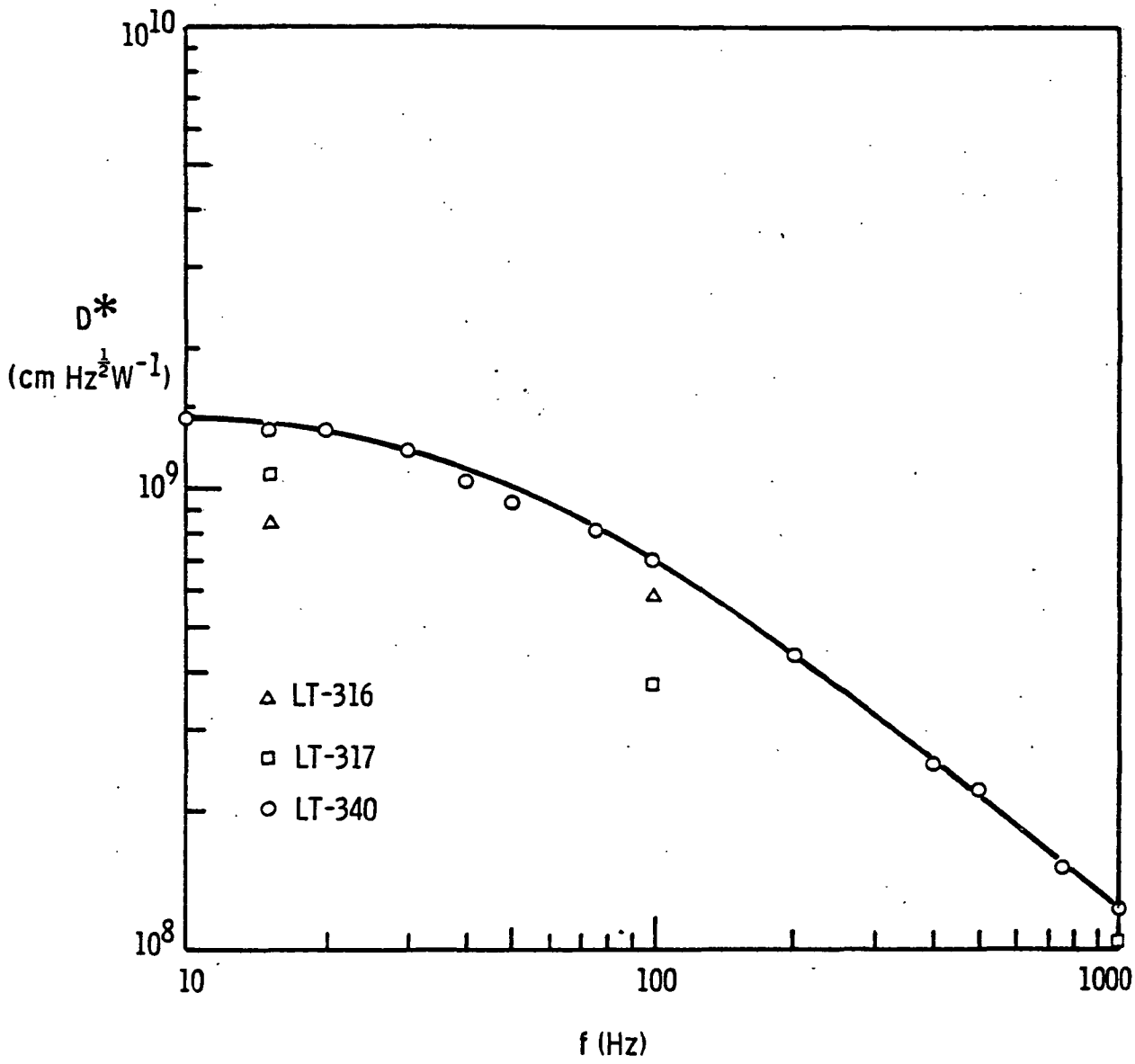

Fig. 19. D* of the detector-preamplifier assemblies LT-346, LT-317, and LT-340 as a function of frequency for assemblies under 40 mtorr pressure

DISCUSSION

DIELECTRIC LOSS AND HEAT TRANSFER

Due to the electrothermal coupling present in pyroelectric materials, the measured dielectric loss, Δ, includes the effects of thermal heat transfer between the detector and its surroundings (ref. 5). In detectors constructed at Martin Marietta Laboratories, the dielectric loss has been attributed primarily to this thermal component (ref. 8).

Thermal heat transfer between the detector element and its surroundings can be described in terms of a complex thermal admittance $Y_T(\omega)$ defined as

$$Y_T(\omega) = -dW/dT = G_T + iB_T \tag{7}$$

where

- dW = the rate of heat flow into the detector volume
- dT = the temperature difference between the detector and its surrounding environment
- G_T = conductance, related to the heat flow in phase with the temperature
- B_T = susceptance, related to the out-of-phase component of heat flow.

For the commonly employed lumped-circuit model for thermal heat transfer (ref. 15), the admittance reduces to a frequency-independent conductance G_T ($B_T = 0$). Using the formalism developed in ref. 15, we obtained the following general relation for the thermal component of dielectric loss, Δ_T:

$$\Delta_T = k_T^2 \, \mathrm{Im} \, \frac{i\omega C^E V}{Y_T + i\omega C^E V} \tag{8}$$

where Im(z) refers to the imaginary component of z.

In terms of G_T and B_T,

$$\Delta_T = k_T^2 \frac{\omega C^E V / G_T}{1 + [(B_T/G_T) + (\omega C^E V/G_T)]^2} \tag{9}$$

where

C^E = heat capacity at constant electric field

V = detector volume.

The electrothermal coupling factor, k_T, is given by

$$k_T^2 = p^2 T / C^E \varepsilon \tag{10}$$

where

p = pyroelectric coefficient

ε = dielectric constant

T = detector temperature

For $LiTaO_3$ at 295 K, $k_T^2 = 7.6 \times 10^{-3}$.

In this section, we will estimate the contribution to Δ from thermal diffusion in the $LiTaO_3$ material for the structure shown in Fig. 2. Heat transfer due to radiation and air conduction is negligible for this structure operated in vacuum and is not considered.

Obtaining an exact solution for the heat flow in the indicated structure, with its very complex boundaries, presents a formidable challenge. However, an approximate closed-form solution can be derived that provides greater insight into the nature of the heat flow. The following assumptions were employed:

1. The detector element (defined by its electrodes) is isothermal for a uniformly absorbed heat flux.
2. The temperature decrease in the material surrounding the detector is described by a one-dimensional heat flow.

An electric transmission line analog is employed to evaluate the heat flow characteristics for this model. In this analog, the electrical capacitance per unit length, C', corresponds to $C^E A$, where A is the cross-sectional area, and the electrical resistance per unit length, R', corresponds to $(KA)^{-1}$, where K is the thermal conductivity. The thermal admittance then corresponds to the electrical input admittance, which, from standard texts (ref. 16), is:

$$Y_T = Y_o \frac{Y_L \cosh \gamma \ell + Y_o \sinh \gamma \ell}{Y_o \cosh \gamma \ell + Y_L \sinh \gamma \ell} \tag{11}$$

where

ℓ = distance from the detector to a material boundary

Y_L = thermal admittance at this boundary

Y_o = characteristic admittance

γ = propagation coefficient.

In terms of thermal parameters,

$$Y_o = (i\omega C'/R')^{1/2} = A(iC^E K)^{1/2} \tag{12}$$

$$\gamma = (i\omega C'R')^{1/2} = (i\omega C^E K)^{1/2} \tag{13}$$

The characteristic admittance may also be written in the following convenient form:

$$Y_o = G_o(1+i) \tag{14}$$

$$G_o = KA/L_T \tag{15}$$

$$L_t = (2\kappa/\omega)^{1/2} \tag{16}$$

$$\gamma = (1+i)/L_T \tag{17}$$

where $\kappa = K/C^E$ is the thermal diffusivity. For $LiTaO_3$, the thermal diffusion length, L_T, is 0.166 mm at 15 Hz.

The validity of this model may be checked for the case of a circular detector element (radius a = 0.57 mm) formed on an infinite $LiTaO_3$ slab of thickness b. For the one-dimensional model,

$$Y_T = Y_o = 2\pi bK\beta\ (1+i) \tag{18}$$

$$\beta = a\ (\omega/\kappa)^{1/2} \tag{19}$$

For a = 0.57 mm and b = 2 μm, we find G_T = 179 μWK^{-1} at 15 Hz.

The exact solution (ref. 17) is

$$Y_T' = 2\pi bK\beta(1+i)\ \frac{K_0(\beta e^{-i\pi/4})}{K_1(\beta e^{-i\pi/4})} \tag{20}$$

$$= Y_o\ K_0(\beta e^{i\pi/4})/K_1(\beta e^{i\pi/4})$$

where K_0, K_1 are modified Bessel functions. For large β, the ratio K_0/K_1 approaches unity. In particular, at 15 Hz, β = 4.8, and $K_0/K_1 = 0.93 \angle 3.6°$. Thus, for frequencies above 15 Hz, the admittances derived from the one-dimensional model agree to within 7% of those derived from the exact solution.

The principle heat conduction path for the structure in Fig. 2 is through the three spokes. Since the length of each spoke, 0.54 mm, is several thermal diffusion lengths (L_T) at frequencies above 10 Hz,

$$G_T = R_T = G_o = KA_s/L_T \tag{21}$$

$$A_s = 3\ w_s b_s \tag{22}$$

where

w_s = spoke width

b_s = spoke thickness.

In this approximation, the conductance is directly related to the cross-sectional area A_s of the supporting spokes. Thus, reticulation reduces the conductance by a factor R, where

$$R = A_s/2\pi ab = \frac{3w_s b_s}{2\pi ab} \tag{23}$$

For the detector design of Fig. 2, R = 0.34 with b_s and b taken as 4 and 2 μm, respectively.

Since the detector is metallized to within a distance ℓ of the rim of the slot, heat flow can occur into the region between element and rim. The admittance can be obtained from eq. (11) with ℓ = 0.030 or 0.060 mm. Since heat flow beyond the rim is negligible, Y_L is taken as zero. Then,

$$Y_T = G_T + iB_T = G_o(1+i)\tanh[(1+i)\ell/L_T] \tag{24}$$

For $\ell/L_T \ll 1$, G_T vanishes and, therefore, by eq. (9), Δ_T also vanishes. For ℓ = 0.03 mm, G_T is less than 5% of the conductance of an unreticulated structure for frequencies less than 50 Hz. Since the low-frequency region is of primary interest, heat transfer into the region between the element and rim will be neglected in this analysis.

The thermal conductance can also be estimated from responsivity data. The voltage response can be derived in terms of the thermal admittance in the same manner as the dielectric loss. R_V is then given by eq. (5) with the normalized response function $I(\omega)$ taken as:

$$I(\omega) = \frac{\omega C^E V/G_t}{[1+(B_T/G_T + \omega C^E V/G_T)^2]^{1/2}} \tag{25}$$

If we assume the admittance has the form

$$G_T = B_T = E\,\omega^{1/2} \tag{26}$$

which is predicted for a spoke conductive structure (see eq. (21)), then E can be determined from a best fit of the responsivity data to eqs. (5), (25), and (26).

The curve in Fig. 17 was fitted in this manner to the R_V data from detector LT-340. The conductance derived from this curve at 15 Hz is 104.6 μWK^{-1}, or 59% of the unreticulated value. Thus, the thermal conductance derived from experiment is 74% larger than the theoretically derived value. The difference may be attributed to the approximate model employed and to possible deviations of the dimensions of LT-340 from those shown in Fig. 2. For example, the spoke thickness, b_s, was found to vary by $\pm$ 1 μm for detectors from the same wafer.

From eq. (9), and experimentally and theoretically derived thermal admittances, the dielectric loss from heat transfer was computed. Fig. 20 compares these calculated losses with Δ_T for an unreticulated structure. Note that at 15 Hz, reticulation reduces Δ_T to 73% of the unreticulated value.

The experimentally determined Δ may be subtracted from the residual loss shown in Fig. 18 to obtain the residual surface conductance loss. This loss together with series resistance, materials, and thermal losses is shown in Fig. 21 for LT-340, from which it can be seen that, in the low-frequency region, 10-100 Hz, the thermal loss is the principal loss, although the loss due to surface conductance is appreciable.

NOISE

To enhance the D* of the detector preamplifier assembly, the output noise voltage of the assembly must be minimized. Thus, the contributing sources of the noise voltage must be derived and evaluated for significance. Selective

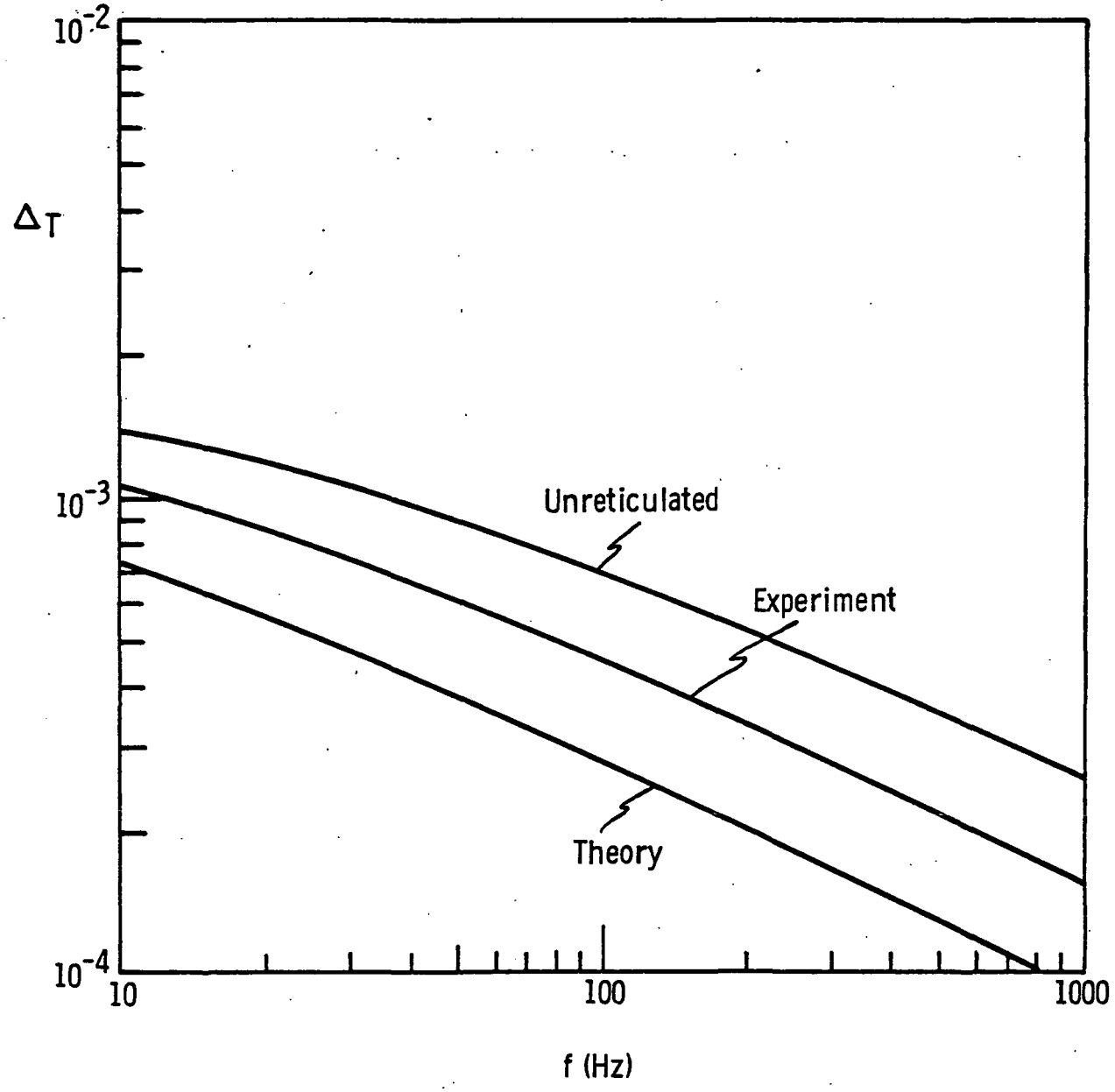

Fig. 20. Thermal component of dielectric loss, Δ_T, computed from the theoretically and experimentally derived thermal admittances and the Δ_T for an unreticulated structure

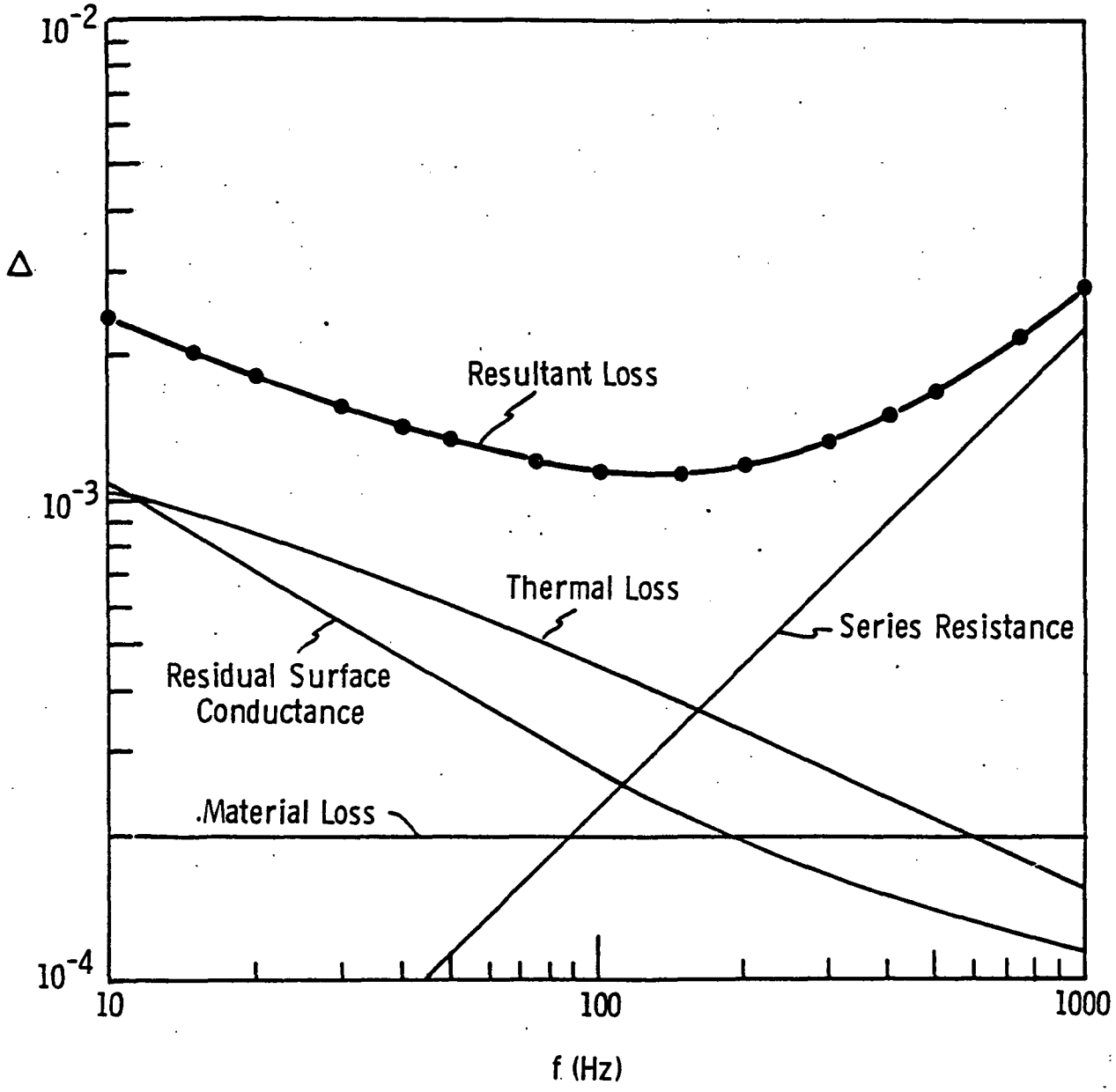

Fig. 21. Detector loss components as a function of frequency measured for LT-340 under 40 mtorr pressure

means can then be devised for their elimination or redressment where possible.

Stated as a noise voltage at the output of the preamplifier, the noise voltage contribution from the dielectric loss of the detector in the frequency limit $\omega R_L C >> 1$ can be written as

$$V_D = g\ (4kTG)^{1/2} \omega C$$

where

k = Boltzmann constant

T = detector temperature

G = ac electrical conductance of the detector.

By writing G in terms of the loss tangent Δ of the detector as in eq. (6) and utilizing the results of the previous section where the detector loss was shown to consist of a material loss, Δ_m, a thermal loss, Δ_T, a series resistance loss, Δ_r, and a residual surface loss, Δ_{SC}, we can state the noise voltage contribution from these losses as

$$V_D = (\Sigma V_i^2)^{1/2} \tag{27}$$

where

$$V_i = g\ (4kT\Delta_i/\omega C)^{1/2} \tag{28}$$

Δ_i = component losses cited above

V_i = corresponding noise voltage contribution (V_m, V_T, V_r, V_{SC}) from the component loss.

The preamplifier has a Johnson noise contribution V_j from the load resistor R_L, which is given by

$$V_j = g\ (4kT/R_L)^{1/2}\ \frac{1}{\omega C} \tag{29}$$

Also, there is an input current noise contribution, V_I, as a result of

the FET gate-leakage current, I_G, given by

$$V_I = g\ (2qI_G)^{1/2}\ \frac{1}{\omega C} \tag{30}$$

where q is the electron charge. Likewise associated with the preamplifier is a FET voltage noise, V_e, due to its channel conductance. As with the FET gate leakage current, V_e was measured in the laboratory and was cited in the manufacturer's specifications.

The leakage conductance, G_C, resulting from assembling the detector and preamplifier produces a noise voltage

$$V_{GC} = g\ (4kTGC)^{1/2}/\omega C \tag{31}$$

The resultant noise voltage, V_N, at the output of the preamplifier can be stated, therefore, as

$$V_N = [\Sigma V_i^2 + V_j^2 + V_I^2 + V_e^2 + V_{GC}^2]^{1/2} \tag{32}$$

In Fig. 22, the theoretical noise voltages calculated from the measured parameters and the losses previously cited in this section are shown along with the noise voltage results for LT-340. The model results agree very well with the measured results and serve as a guide in assessing methods of noise reduction.

At 15 Hz, the major contributing noise sources are those due to the thermal loss, the residual surface loss, and the loss related to the leakage conductance of the assembly. Further reductions in thermal loss are limited by the support requirements of the detector, i.e., although reticulation reduces the paths of thermal loss, the structural integrity of the device must be maintained. Furthermore, low temperature operation (4°C) offers little advantage since V_T is directly related to the absolute temperature (eqs. (10) and (28)).

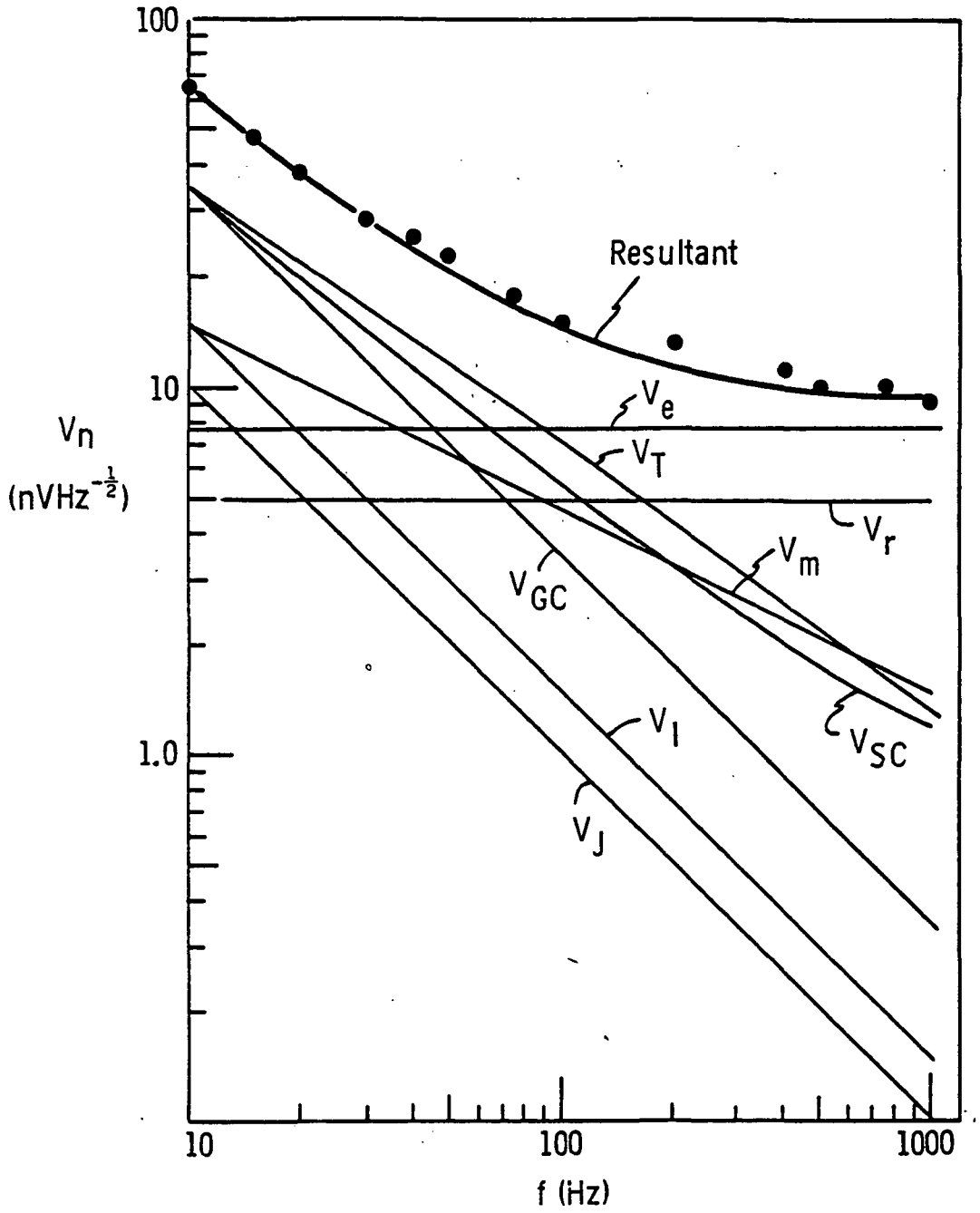

Fig. 22. Noise voltage components as a function of frequency measured for LT-340 assembly under 40 mtorr pressure

The surface loss and the assembly conductance, however, are due to leakage conductances which are redressable by improved processing procedures, such as ion milling, and by cleaning the detector-preamplifier assembly. The elimination of these noise voltages would be significant in reducing the resultant noise voltage at 15 Hz. Further reductions in the resultant noise voltage due to reducing the FET gate leakage current and the FET noise voltage are relatively insignificant compared with the remaining thermal loss contribution V_T. As can be deduced from Fig. 22, only 4% additional reduction can be achieved by eliminating V_I.

The elimination of V_{sc} and V_{GS} alone would produce a reduction in the noise voltage at 15 Hz of 30%. With an absorptance of 80% as cited in "Test Results" and a 33.8 $\mu V/Hz^{1/2}$ noise voltage, which would follow the elimination of V_{sc} and V_{GC} in Fig. 22, a D* of 2.8×10^9 $cmHz^{1/2}W^{-1}$ for the detector appears feasible.

CONCLUSIONS

The results of this program have demonstrated that the detectivity of lithium tantalate pyroelectric detectors can be improved by the use of AR coatings to increase absorptivity, by reticulation to reduce temperature noise, and by thinning detector elements to less than 3 μm. It has also been shown that it is possible to construct hybrid preamplifiers with noise levels small compared to detector noise. Operation at reduced pressures was found to reduce noise (primarily temperature noise) and increase responsivity. However, cooling detectors to 4°C produced little decrease in noise.

Further improvements in D* can be readily achieved by fitting the detector with the optimized AR coating designed late in this program, and by reducing leakage conductances on the detector through ion mill cleaning. A detectivity of D* (500 K, 15 Hz) = 2.8×10^9 $cmHz^{1/2}W^{-1}$ is anticipated through these modifications. Improvements beyond this level accrue at the expense of structural integrity, i.e., D* can be enhanced by reducing supporting spoke thickness and by further thinning the element, but such a fragile device would be of little practical value. Thus, detectivities on the order of 2.5×10^9 $cmHz^{1/2}W^{-1}$, which can be achieved with techniques developed under this contract, represent a practical limit for $LiTaO_3$ pyroelectric detectors.

The vibration sensitivities of the units fabricated were comparable to those we have obtained with unreticulated structures. Further reductions in vibrational sensitivity with minimum responsivity loss can be achieved using the complementary structure.

Langley Research Center

National Aeronautics and Space Administration

Hampton, Virginia 23665

November 1, 1978

REFERENCES

1. Beerman, H.P.: Pyroelectric Infrared Radiation Detector. Am. Ceram. Soc. Bull., vol. 46, 1967, p. 737.

2. Roundy, C.B.; and Byer, R.L.: Sensitive $LiTaO_3$ Pyroelectric Detector. J. Appl. Phys., vol. 44, 1973, p. 929.

3. Glass, A.M.: Investigation of Electrical Properties of $Sr_{1-x}Ba_xNb_2O_6$ with Special Reference to Pyroelectric Detection. J. Appl. Phys., vol. 40, 1969, p. 4699.

4. Phelan, R.J., Jr.; Mahler, R.J.; and Cook, A.R.: High D* Pyroelectric Polyvinylfluoride Detectors. Appl. Phys. Letters, vol. 19, 1971, p. 337.

5. Lock, P.J.: Doped Triglycine Sulfate for Pyroelectric Applications. Appl. Phys. Letters, vol. 19, 1971, p. 390.

6. Byer, N.E.; Stokowski, S.E.; and Venables, J.D.: Complementary Domain Pyroelectric Detectors with Reduced Sensitivity to Mechanical Vibrations and Temperature Changes. Appl. Phys. Letters, vol. 27, 1975, p. 639.

7. Liu, S.T.: Critical Assessment of Pyroelectric Detectors. Ferroelectrics, vol. 10, 1976, p. 83.

8. Stokowski, S.E.; and Byer, N.E.: Temperature Noise-Limited Pyroelectric Detectors. Proceedings of the International Electron Device Meeting. Washington, D.C., IEEE, 1976, p. 555.

9. Stokowski, S.E.; Venables, J.D.; Byer, N.E.; and Ensign, T.C.: Ion-beam Milled, High Detectivity Pyroelectric Detectors. Infrared Physics, vol. 16, 1976, p. 331.

10. Putley, E.H.: The Pyroelectric Detector. Semiconductors and Semimetals, vol. 5. Willardson and Beer, eds., Academic Press, New York, 1970, pp. 259-285.

11. Ramsey, W.Y.: Specular Spectral Reflectance of Paints from 0.4 to 40 Microns. Meteorological Satellite Laboratory Report No. 31, U.S. Dept. of Commerce Weather Bureau, Washington, D.C., 1964.

12. Roundy, C.B.; and Byer, R.L.: Subnanosecond Pyroelectric Detector. Appl. Phys. Letters, vol. 21, 1972, p. 512.

13. Heavens, O.S.: Optical Properties of Thin Solid Films. Butterworths Scientific Publications, London, 1955.

14. Pyroelectric Detector with Decreased Susceptibility to Vibrational Noise. U.S. Patent 4,060,729, Nov. 1977.

15. Stokowski, S.E.: Temperature Noise and Dielectric Loss in Pyroelectric Detectors. Appl. Phys. Letters, vol. 29, 1976, pp. 393-395.

16. Ramo, S.; and Whinnery, J.R.: Fields and Waves in Modern Radio. John Wiley & Sons, Inc., New York, 1953, pp. 38-42.

1. Report No.	2. Government Accession No.	3. Recipient's Catalog No.
NASA CR-158982		

4. Title and Subtitle	5. Report Date
Development of Improved Lithium Tantalate Pyroelectric Detectors	November 1978
	6. Performing Organization Code ---
7. Author(s)	8. Performing Organization Report No.
N. E. Byer, A. Van der Jagt, and W. Holton	TR78-49
	10. Work Unit No.
9. Performing Organization Name and Address	11. Contract or Grant No.
Martin Marietta Corporation Martin Marietta Laboratories 1450 South Rolling Road Baltimore, Maryland 21227	NAS1-15106
	13. Type of Report and Period Covered
12. Sponsoring Agency Name and Address	Final Report 9/14/77 - 9/30/78
National Aeronautics and Space Administration Washington, D.C. 20546	14. Sponsoring Agency Code

15. Supplementary Notes

Langley Technical Monitor: Dr. James B. Robertson

16. Abstract

A program was undertaken to increase the detectivity of $LiTaO_3$ pyroelectric detectors to meet a performance requirement of $D^*(500\ K, 15\ Hz)=4x10^9\ cmHz^{1/2}W^{-1}$. Emphasis was placed on reduction of the thermal conductance of the detector element to its surroundings, thinning the detector wafer to a thickness less than 3 μm, and increasing the absorptivity of the standard metallic film coatings.

During the program, thermal conductance was reduced 41% through the use of reticulated (slotted) structures. Self-supported detector wafers less than 2 μm thick were fabricated. Multiple layer coatings, including an AR coating, with 16% more absorptance, were designed and fabricated. Later refinements in the multilayer design program gave absorptivities of 75-80%, but detectors with these coatings had to be more than 2 μm thick because of a mismatch in the thermal expansion coefficients with $LiTaO_3$.

Three assemblies were constructed and delivered, consisting of the detector chip (with standard nichrome coatings) and a hybrid JFET preamplifier sealed in an evacuable header with a germanium window. A $D^*(500\ K, 15\ Hz)$ of $1.34x10^9\ cmHz^{1/2}W^{-1}$ was achieved in a vacuum ambient. Vibrational sensitivities were 20-60 μV/g, comparable to those of unreticulated devices. Based on this program, $D^* = 2.5x10^9\ cmHz^{1/2}W^{-1}$ can be contemplated, but practical $LiTaO_3$ detectors with larger D^* are unlikely.

17. Key Words (Suggested by Author(s))	18. Distribution Statement
infrared detector, pyroelectric detector, lithium tantalate, ion beam milling, absorptive coatings, wagon wheel construction, bath tub construction, thin film coatings, metallic coatings	Unclassified - Unlimited

19. Security Classif. (of this report)	20. Security Classif. (of this page)	21. No. of Pages	22. Price*
Unclassified	Unclassified	67	

* For sale by the National Technical Information Service, Springfield, Virginia 22161